communications biology

Article

https://doi.org/10.1038/s42003-024-06630-7

Macroscale brain states support the control of semantic cognition

Xiuyi Wang [1,2,3] ✉, Katya Krieger-Redwood[3], Yanni Cui[1], Jonathan Smallwood [4], Yi Du [1,2,5,6] ✉ & Elizabeth Jefferies [3] ✉

A crucial aim in neuroscience is to understand how the human brain adapts to varying cognitive demands. This study investigates network reconfiguration during controlled semantic retrieval in differing contexts. We analyze brain responses to two semantic tasks of varying difficulty – global association and feature matching judgments – which are contrasted with non-semantic tasks on the cortical surface and within a whole-brain state space. Demanding semantic association tasks elicit activation in anterior prefrontal and temporal regions, while challenging semantic feature matching and non-semantic tasks predominantly activate posterior regions. Task difficulty also modulates activation along different dimensions of functional organization, suggesting different mechanisms of cognitive control. More demanding semantic association judgments engage cognitive control and default mode networks together, while feature matching and non-semantic tasks are skewed towards cognitive control networks. These findings highlight the brain's dynamic ability to tailor its networks to support diverse neurocognitive states, enriching our understanding of controlled cognition.

Adaptive behavior hinges on understanding the meanings of our surroundings and modulating our responses accordingly. While research has focused on how the brain stores semantic information and controls cognition to achieve our goals, fewer studies have investigated the intersection of these domains to understand how we flexibly retrieve context-appropriate information. For example, searching for your dog on a crowded beach might focus on visual features like color and shape. In contrast, at a family gathering, associative details become more relevant – recognizing that dogs are strongly food-motivated, and chocolate is harmful to them. These scenarios highlight our ability to adapt semantic retrieval to different situations. However, current descriptions of brain networks underpinning conceptual representation and control fall short in explaining how we generate diverse brain states (i.e., patterns of brain activity or functional coupling that reflect different types of cognitive processes), which can support these different retrieval patterns.

Semantic cognition relies on conceptual representations distilled from sensory-motor features within heteromodal hub(s), including anterior temporal cortex, as well as two networks that support cognitive control – semantic control network (SCN) and multiple demand network (MDN)[1,2]. MDN, particularly its frontoparietal regions including the bilateral inferior frontal sulcus and intraparietal cortex, responds to executive demands across various tasks[3–6]. It is thought to support domain-general control processes, such as maintaining goals applicable to different types of representations, including semantic information[3]. Concurrently, SCN is partially-overlapping yet dissociable, including the left inferior frontal gyrus (IFG), posterior temporal cortex, and dorsomedial prefrontal cortex[7,8]. It is engaged in controlled, flexible semantic retrieval but not demanding non-semantic tasks[9–12].

Given that the MDN is recruited across various domains and the SCN is implicated in diverse semantic tasks, a pivotal question arises: How do we generate whole-brain states—i.e., patterns of correlation and anti-correlation across brain regions that relate to the configuration of large-scale networks—which allow us to focus on different aspects of knowledge appropriate for a specific task context[13]? The relationship between these two control networks provides a clue. Although proximal on the cortical surface, for example, in the left lateral prefrontal cortex, they occupy distinct positions in a hierarchy from sensory-motor to heteromodal cortex[11,12]. This proximity might explain why controlled semantic retrieval elicits stronger responses in the left anterior lateral prefrontal cortex, while tasks involving non-semantic control effects and semantic feature matching activate the posterior lateral prefrontal cortex[14–17]. These functional differences might reflect the principal dimension of intrinsic connectivity, which accounts for the largest variance in resting-state fMRI and differentiates between heteromodal and unimodal processing. Prior research suggests that the SCN is

[1]CAS Key Laboratory of Behavioral Science, Institute of Psychology, Chinese Academy of Sciences, Beijing, 100101, China. [2]Department of Psychology, University of Chinese Academy of Sciences, Beijing, 100049, China. [3]Department of Psychology, University of York, Heslington, York, YO10 5DD, UK. [4]Department of Psychology, Queens University, Kingston, Ontario, Canada. [5]Chinese Institute for Brain Research, Beijing, 102206, China. [6]CAS Center for Excellence in Brain Science and Intelligence Technology, Shanghai, 200031, China. ✉e-mail: wangxiuyi@psych.ac.cn; duyi@psych.ac.cn; beth.jefferies@york.ac.uk

closer to the heteromodal end of this dimension than the MDN[11]. Consequently, we hypothesize that the difficulty effects in semantic association and semantic feature matching will not only show topographical differences in the left lateral prefrontal cortex but that these differences will extend to anterior and posterior areas of the posterior temporal and medial prefrontal areas, where the SCN and MDN are adjacent[7,8]. Should this hypothesis be validated, it would elucidate how the functional architecture of the brain varies according to the cognitive demands of semantic tasks. It would indicate that adjacent, yet functionally distinct large-scale neural networks are systematically organized on the brain's surface, supporting different facets of semantic control. This would support the contemporary understanding that cortical geometry, or the spatial layout of brain regions, critically influences their functions[17–19].

Different states of controlled cognition (i.e., the varying functional states of the brain as it engages in different cognitive activities and specific tasks) may reflect specific configurations of large-scale brain networks, which can be characterized in terms of multiple dimensions of intrinsic connectivity[18,20]. In addition to the principal dimension of intrinsic connectivity differentiating heteromodal from unimodal processing, a second dimension separates visual from auditory-motor processes, while a third dimension delineates the functional separation between cognitive control systems and the memory system supported by the Default Mode Network (DMN)[18,20]. The DMN comprises a set of widely distributed brain regions in the parietal, temporal and frontal cortex, including the ventral medial prefrontal cortex, the dorsal medial prefrontal cortex, the posterior cingulate cortex and adjacent precuneus, the lateral parietal cortex, and the entorhinal cortex. These regions play a pivotal role when cognition relies on information from memory[19,21–23]: DMN is active during periods of future thinking[24], the application of acquired task rules[23], semantic decisions that depend on strong conceptual associations[25], and during spatial or numerical decisions made based on memory rather than perceptual input[26,27].

When controlled semantic retrieval is required to establish relevant thoughts and behaviors without an externally-imposed goal (e.g., focusing on globally weak associations relevant to the context), heteromodal regions that support long-term semantic knowledge are thought to integrate with control processes tailored to the circumstances[11,25,28,29]. Conversely, states of top-down control and selection, which are prevalent in feature matching, often involve anti-correlation between control networks and DMN[11,19]. Semantic feature matching judgments are thought to rely on a domain-general selection process that operates post-retrieval to resolve competition among active representations[14–17]. This process might demand the engagement of domain-general control mechanisms together with sensory-motor systems, necessitating the separation of DMN from executive networks within heteromodal cortex. These distinctions motivated us to predict that different cognitive tasks would employ varied neural mechanisms and control strategies (i.e., brain states), with the feature matching task aligning more closely with non-semantic control functions than the retrieval of weak associations. By mapping controlled activation patterns within a whole-brain state space defined by the first three dimensions of variation in intrinsic connectivity, we can elucidate spatial activation differences across the whole brain based on their reliance on heteromodal versus unimodal cortex, visual versus auditory-motor inputs, and the extent of control network engagement independent of DMN. Consequently, this approach allows us to understand diverse patterns of network interactions across different task contexts.

In this study, we explored how networks implicated in control are engaged on the cortical surface and in a whole-brain state space defined by the top three dimensions of intrinsic connectivity. To achieve this, we varied the demands of two semantic tasks—global association and semantic feature matching—and contrasted the effects of control with those of two non-semantic tasks, spatial working memory and math judgments. Our study had three primary objectives: (i) To establish if brain regions supporting controlled retrieval of semantic associations are anterior to those for visual feature selection (cf. [14]), not only within left inferior frontal gyrus but also in medial prefrontal and posterior temporal cortex, indicating an organized topographical dissociation in whole-brain organization. (ii) To determine whether control processes linked to semantic feature matching overlap more with non-semantic control regions than those engaged in the controlled retrieval of semantic associations. (iii) To understand the organization of cognitive control in neural state space, in which differences in activation are interpreted in terms of dimensions of whole-brain functional organization. Thus, our research builds on prior findings of multiple control networks (SCN versus MDN) and functional dissociations within LIFG, to establish whether multiple modes of controlled cognition are underpinned by distinct dimensions of neural organization.

We found demanding semantic association tasks elicited more activation in the anterior regions of prefrontal and temporal cortex. In contrast, difficult semantic feature matching tasks produced more posterior activation, aligning closely with regions engaged during challenging non-semantic tasks. In both semantic feature matching and non-semantic contexts, difficulty effects were situated towards the controlled end of a dimension capturing functional separation between cognitive control and default mode regions, while difficulty effects for association judgments were located towards the heteromodal end of a dimension capturing functional separation between heteromodal and unimodal cortex. In this way, we found a variety of brain states underpinned controlled cognition even when tasks were superficially matched—i.e., utilizing identical stimuli and with the same presentation and response format, such that the primary distinction between these tasks concerned the nature of the controlled retrieval process. Specifically, cognitive control regions were found to interact with the heteromodal semantic knowledge system when identifying contextually relevant conceptual overlap (e.g., associating 'DOG' with 'BEACH'), while these control and long-term memory systems separated in tasks requiring cognition to be focused on specific overlapping features (e.g., connecting 'DALMATIAN' with 'COW' via the feature 'BLACK AND WHITE').

Results

This study analyzed two datasets collected at the University of York, UK. The first dataset involved two semantic control tasks[19], while the second dataset involved two non-semantic control tasks, aimed at localizing the MDN[11,30]. A recent study employing the same dataset focused on subnetworks within the frontoparietal control subnetwork and showed different activation patterns across these semantic and non-semantic tasks[19]. The current study instead explores how networks are engaged on the cortical surface and in whole-brain state space, and specifically examines parametric variations in task difficulty within the two semantic tasks. This allows us to establish how the difficulty of semantic association and feature matching tasks activate different brain regions and rely on distinct brain states, even when these tasks are superficially highly similar.

Behavioral data

Semantic tasks. We parametrically manipulated the difficulty of two semantic tasks (Fig. 1). In these tasks, participants decided whether a word pair shared a semantic relationship by making Yes/No decisions based on either: (i) association strength, accessing whether two concepts were globally related in meaning; or (ii) feature overlap, evaluating whether two concepts shared similar visual features (either color or shape). The semantic association task presented word pairs with varying degrees of association. Stronger associations were expected to facilitate decision making for related ("Yes") trials, since they are typically more easily accessible from the semantic long-term store. Conversely, relatively strong associations could complicate unrelated ("No") decisions (see Supplementary section 1.2). In this task, participants were not given an explicit goal or specific instructions on how to link the concepts but were asked to make decisions based on overall semantic similarity. This design directed controlled retrieval towards aspects of the concepts that matched a shared context, with information from the semantic store providing this context.

In the semantic feature matching task, in contrast, participants were asked to decide if two concept words shared a specific visual feature—color

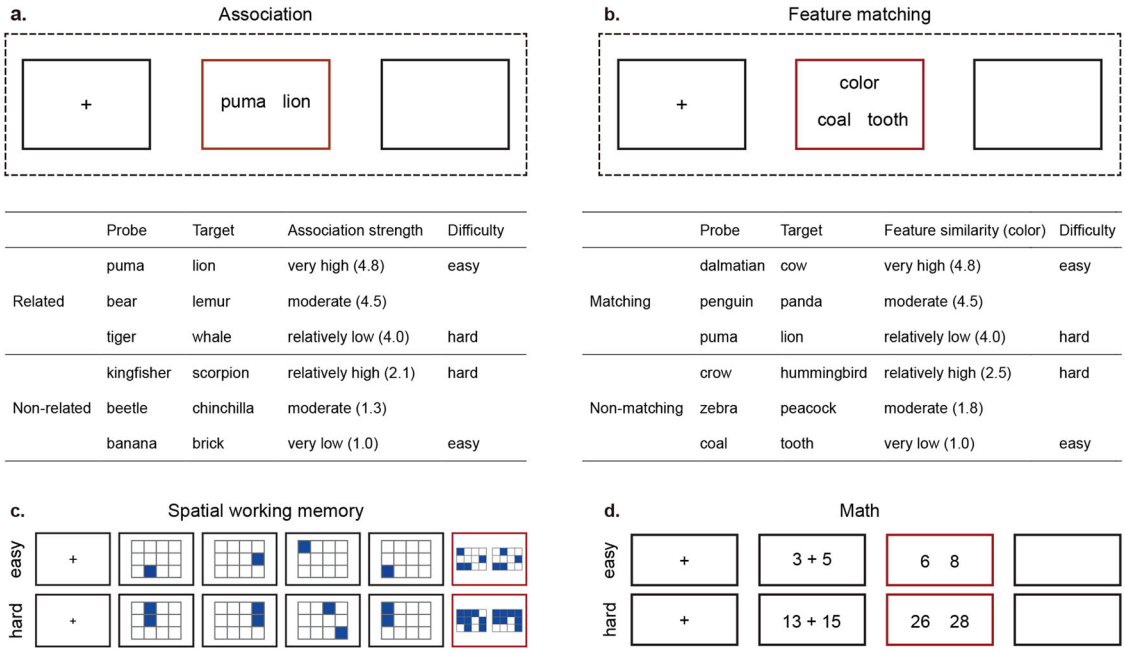

	Probe	Target	Association strength	Difficulty
Related	puma	lion	very high (4.8)	easy
	bear	lemur	moderate (4.5)	
	tiger	whale	relatively low (4.0)	hard
Non-related	kingfisher	scorpion	relatively high (2.1)	hard
	beetle	chinchilla	moderate (1.3)	
	banana	brick	very low (1.0)	easy

	Probe	Target	Feature similarity (color)	Difficulty
Matching	dalmatian	cow	very high (4.8)	easy
	penguin	panda	moderate (4.5)	
	puma	lion	relatively low (4.0)	hard
Non-matching	crow	hummingbird	relatively high (2.5)	hard
	zebra	peacock	moderate (1.8)	
	coal	tooth	very low (1.0)	easy

Fig. 1 | Illustration of the semantic and non-semantic tasks. a Semantic association task: Participants made yes/no decisions about whether pairs of words were globally semantically associated or not. We parametrically manipulated the association strength between the probe and target word, typically judged to be related or unrelated on a 5-point rating scale. **b** Semantic feature matching task: Participants decided if probe and target concepts shared a specific visual semantic feature (color or shape), indicated at the top of the screen during each trial. The feature prompt, probe and target words appeared simultaneously. We parametrically manipulated the degree of feature similarity between the probe and target concepts that were typically judged to be matching or non-matching for the specified feature on a 5-point rating scale. **c**, **d** Non-semantic tasks for domain-general control: **c** involved a spatial working memory task where participants tracked sequentially presented locations. **d** entailed math decision tasks, requiring the maintenance and manipulation of single or double-digit numbers.

or shape. The word pairs parametrically varied in feature similarity—i.e., how similar the concepts were in terms of the feature being matched. A high degree of feature similarity was anticipated to ease the decision-making for matching ("Yes") trials, as it would likely increase participants' confidence in their matching decisions. Conversely, lower feature similarity was expected to simplify non-matching ("No") trials, making the basis for non-matching decisions more apparent (see Supplementary section 1.3). Unlike the semantic association task, the semantic feature matching task explicitly required participants to focus on and execute a specific semantic goal for semantic retrieval, making broader conceptual information about the concepts irrelevant.

Our first analysis verified the effectiveness of our parametric manipulation of task demands. To examine how semantic association strength influenced response time (RT) in the semantic association task, we built a linear mixed effect model. This model accounted for individual differences in the difficulty effect by including random intercepts and slopes. We compared a model incorporating a linear effect of semantic association strength with a model without this effect. The results showed that association strength significantly facilitated decision making for related trials ($z = -9.244$, $p < 0.0001$) but had no discernible effect on unrelated trials ($z = 0.018$, $p = 0.986$), after controlling for feature similarity and global similarity, the latter being the overall similarity of each word pair as rated by an independent group of 30 participants (Fig. 2a). We conducted a comparable analysis for the feature matching task to investigate how feature similarity influenced response times and accuracy. The results indicated that higher feature similarity facilitated decision-making for matching trials (RT: $z = -10.51$, $p < 0.0001$), but impeded decisions for non-matching trials (RT: $z = 11.97$, $p < 0.0001$) after controlling for association strength and global similarity (Fig. 2b). To maintain clarity in our visual presentation, Fig. 2 instead displays Pearson correlations that illustrate the relationships between association strength and response time, feature similarity and response time, and feature similarity and accuracy. Although these visualizations stem from a different statistical approach, they support the conclusions of the linear mixed-effects models.

Non-semantic tasks. To investigate the overlap between effects of semantic control in the two semantic tasks and domain-general cognitive control, we included two non-semantic tasks commonly used to localize regions of the MDN: a spatial working memory task and a math task[4]. In the spatial working memory task, participants tracked locations presented in sequence, with the easy version involving one location per slide and the hard version two locations, thus increasing working memory load. In the more demanding version, both accuracy and RT were affected, showing decreased accuracy ($t(26) = -8.97$, $p = 7.31 * e{-10}$) and increased RT ($t(26) = 7.14$, $p = 7.20 * e{-8}$) compared to easier trials. Similarly, the math task ranged from single-digit additions in the easy version to double-digit additions in the hard version. The more demanding condition resulted in lower accuracy ($t(26) = -6.73$, $p = 2.19 * e{-7}$) and longer RTs ($t(26) = 12.06$, $p = 8.04 * e{-13}$) compared to easier trials. These contrasts between hard and easy versions of the tasks have been utilized to identify MDN regions responsive to cognitive control demands[4,11,30].

Effects of strength of association and feature similarity on brain responses

Next, we evaluated whether our difficulty manipulations in the semantic association and feature matching tasks engaged common or distinct brain regions using the individual-specific parcellation (Fig. 3e). First, we investigated whether the spatial differences in the left IFG previously reported—more anterior activation for global association matching and more posterior for feature matching[14]—would be replicated with our parametric difficulty manipulation in these two tasks. Secondly, we explored whether this functional dissociation extended to other brain areas, such as the left posterior temporal and medial prefrontal regions. Confirmation of this would indicate that adjacent yet functionally distinct large-scale neural networks

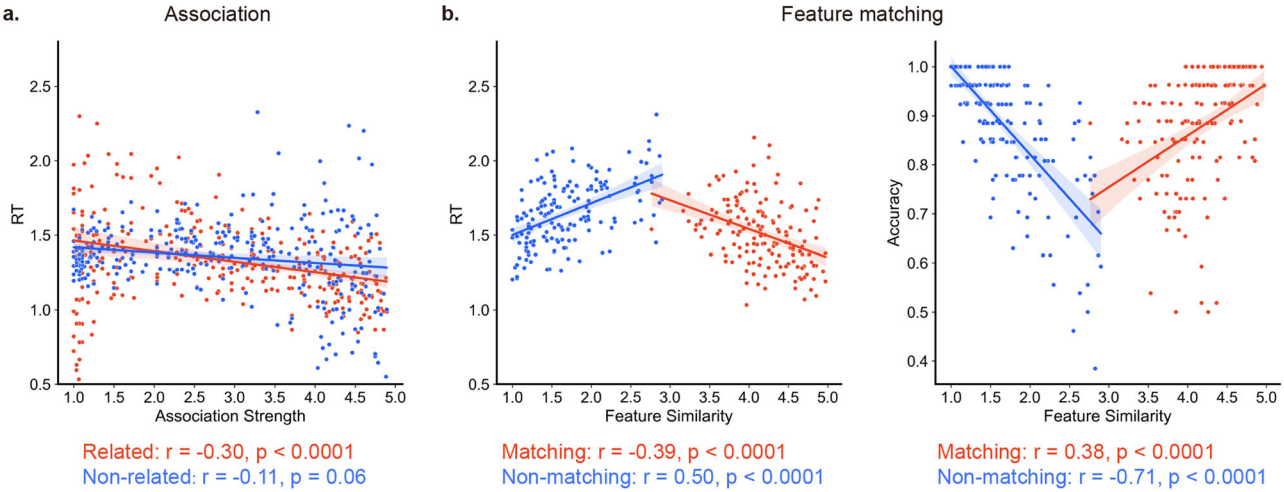

Fig. 2 | Behavior data for the semantic tasks. a In the semantic association task, semantic association strength was negatively correlated with response time for the related trials, but had no significant correlation for the unrelated trials. **b** In the feature matching task, feature similarity was negatively correlated with RT for the matching trials, but positively correlated for the non-matching trials. In the feature matching task, feature similarity showed a positive correlation with accuracy for matching trials, but a negative correlation for the non-matching trials. An analysis of accuracy for the association matching task was not performed because participants made their own judgements about which words were related and which were unrelated. For trials with intermediate association strengths, these decisions vary across individuals.

are systematically organized on the brain's surface, with each supporting different facets of semantic control.

We pinpointed brain regions that exhibited a stronger response to more difficult trials in the two semantic tasks. This increase in activation occurred when (i) association strength was lower for related 'Yes' trials or higher for unrelated 'No' trials in the semantic association task, and (ii) feature similarity was lower for matching 'Yes' trials or higher for non-matching 'No' trials in the feature matching task. We also identified regions that showed greater activation in easier trials. The main task effects (i.e., greater activation during the task relative to the resting baseline) are shown in the Supplementary section 1.1 and Supplementary Fig. 1.

Figure 3a shows the parametric manipulation of semantic association strength ($p < 0.05$, FDR-corrected), and Fig. 5e shows the corresponding unthresholded map. Multiple regions showed positive effects of decision difficulty, with increased BOLD response when association judgements were more difficult, including temporal-occipital cortex, intraparietal sulcus, inferior frontal sulcus and pre-supplementary motor area (Fig. 3a). Negative effects of this variable, reflecting a stronger BOLD response during easier association judgments, were found in default mode network regions in lateral anterior-to-mid temporal cortex, angular gyrus, and medial and superior frontal regions (Fig. 3a). The unthresholded maps for difficulty effects in related and unrelated trials were spatially similar (Supplementary Fig. 2, i.e., the effects of weaker associations when items were judged to be related and stronger associations when items were judged to be unrelated were significantly correlated using spin permutation).

Figure 3b shows the thresholded difficulty effect of feature similarity ($p < 0.05$, FDR-corrected) and Fig. 5f shows the corresponding unthresholded map. Positive effects of decision difficulty across matching and non-matching trials (i.e., stronger responses to harder trials) were found in the regions of domain general control (Fig. 3f), including inferior frontal sulcus, pre-supplementary motor area, temporal-occipital cortex, and intraparietal sulcus (Fig. 3b). Conversely, regions in the DMN (Fig. 3f) showed negative effects of decision difficulty (i.e., stronger responses to easier trials), including lateral anterior-to-mid temporal cortex, angular gyrus, medial and superior frontal regions, and posterior cingulate cortex (Fig. 3b). The unthresholded maps for difficulty effects in matching and non-matching trials were spatially similar (Supplementary Fig. 2; i.e., the effects of lower similarity for matching trials and higher similarity for non-matching trials were correlated using spin permutation).

Although there was considerable overlap in the effect of difficulty for association strength and feature similarity (Fig. 3c), there were also differences in difficulty effects across tasks (Fig. 3d). A direct comparison of the parametric difficulty effects in semantic association and feature matching tasks revealed stronger modulation by difficulty in the semantic association task within DMN regions, including the posterior cingulate cortex, ventral prefrontal cortex, and temporal pole (Fig. 3d). This aligns with the view that the semantic association task more intensively engages controlled retrieval from heteromodal regions. Conversely, stronger modulation by difficulty in the semantic feature matching task was found in cognitive control regions, such as the intraparietal sulcus, inferior parietal lobule, and temporal-occipital cortex showed (Fig. 3d). We found that responses to difficulty in global association judgements were more anterior compared to feature matching in the left lateral prefrontal, medial prefrontal, and left posterior temporal cortex (although the anterior-posterior distinction in the medial prefrontal cortex was relatively weak given the absence of difficulty effects specific to feature matching within this region; Fig. 3c). These findings demonstrate that task difficulty can be differentiated not only by activation within individual regions but also by whole-brain topography. The increased demand in feature matching trials might rely more on the controlled retrieval of sensory information to focus on specific visual features of a concept, thus eliciting stronger activation in the lateral and polar occipital cortex. Conversely, more difficult semantic association tasks may predominantly depend on the controlled retrieval of heteromodal long-term knowledge, as they require establishing a linking context for the two words based on general semantic information. This could explain the more anterior response in regions more physically further from the sensory-motor cortex.

Comparison of semantic and non-semantic task demands

To assess the overlap between difficulty effects in semantic tasks and brain regions responsive to non-semantic task demands, we conducted three analyses. First, we compared hard with easy versions of spatial working memory and math judgements (thresholded maps in Fig. 4a, b, unthresholded maps in Fig. 6a, b). Figure 4c, d illustrates the extent of overlap between the difficulty effects of semantic tasks and non-semantic tasks. Specifically, 32% of brain regions in the semantic association task overlapped with non-semantic control regions that showed hard versus easy activation in either spatial working memory or math tasks (turquoise in Fig. 4c), while 71% of parcels in the semantic feature matching task showed

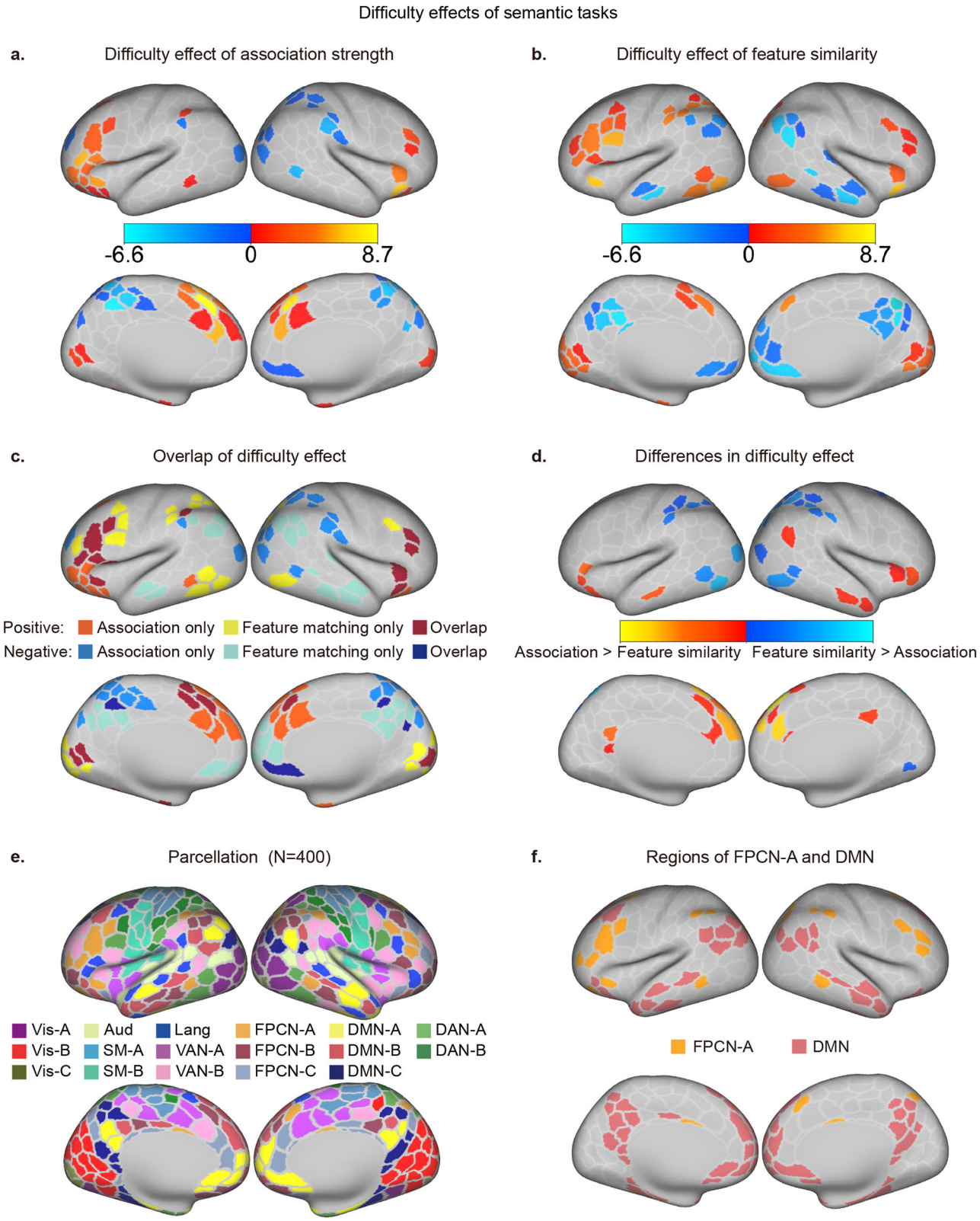

this pattern of overlap (green in Fig. 4d). Next, we defined MDN regions by pinpointing areas that showed a difficulty effect in both spatial working memory task and math task (Fig. 4e). We then compared the activation associated with task difficulty in these MDN regions for the semantic association and semantic feature matching tasks. The difficulty effect was more pronounced for feature similarity than for association strength ($t(27) = 7.28$, $p = 9.91 \times 10$ e−8; Fig. 4e). Finally, we computed spatial correlations between unthresholded difficulty effect maps for non-semantic tasks (Figs. 6a and 6b) and semantic tasks (Fig. 5e, f) and compared these correlations. Non-semantic difficulty showed stronger positive correlation with task demands in feature matching (spatial working memory: left hemisphere (LH): $r = 0.72$, right hemisphere (RH): $r = 0.60$; math task: LH:

Fig. 3 | The parametric difficulty effects of semantic association and feature similarity, and their comparison. a The effect of decision difficulty in the semantic association task. Warm colors indicate regions with increased activation during more difficult trials (i.e., weaker association strength in associated trials and stronger in non-associated trials; $p < 0.05$, FDR-corrected). Cold colors represent the regions that showed the reverse trend (i.e., showing greater activation in less demanding trials; $p < 0.05$, FDR-corrected). **b** The effect of decision difficulty in the semantic feature matching task. Warm colors mark regions with heightened activation for more difficult trials (i.e., lower feature similarity in matching trials and higher in non-matching trials). Cold colors denote regions showing the opposite trend. **c** Overlap in decision difficulty effects for these two tasks. For semantic association, increased difficulty elicited stronger activation in anterior cortex, while in feature similarity, it led to stronger engagement in posterior cortex. **d** The comparison of the difficulty effects in these two tasks. Warm colors denote regions more strongly modulated by association strength compared to feature similarity, and cold colors indicate areas showing the opposite pattern. **e** Individual-specific parcellation divided the whole brain into 400 parcels across 17 networks[68]. **f** The regions of the domain-general control network – FPCN-A[19] and DMN which includes its three subnetworks. Vis Visual, Aud Auditory, SM Sensory-motor, DAN Dorsal attention network, VAN Ventral attention network, FPCN Fronto-parietal control network, Lang Language, DMN Default mode network.

$r = 0.68$, RH: $r = 0.62$; all p values = 0) than in semantic association (spatial working memory: LH: $r = 0.31$, RH: $r = 0.08$; math: LH: $r = 0.21$, RH: $r = 0.05$), with significant differences between these correlations (differences with spatial working memory: LH: $z = 5.83$, RH: $z = 6.08$; differences with math: LH: $z = 6.11$, RH: $z = 6.70$; all p values = 0). All p-values were FDR-corrected following spin permutation. These findings confirm that the difficulty effect in the feature matching task overlapped more with neural processes implicated in non-semantic control than the semantic association task.

We further examined if the difficulty of semantic association difficulty elicits more anterior brain responses within parcels more physically distant from sensory-motor cortex than semantic feature matching. We analyzed the proximity of these responses to the sensory-motor cortex (Fig. 3). We categorized parcels into four distinct groups based on their response to difficulty: (i) parcels responsive to difficulty solely during the semantic association task (orange in Fig. 4c), (ii) parcels showing difficulty effects in both semantic association and non-semantic tasks (turquoise in Fig. 4c), (iii) parcels showing difficulty effects in both feature matching and non-semantic tasks (green in Fig. 4d), and (iv) parcels responsive only to difficulty during the semantic feature matching task (yellow in Fig. 4d). We then computed the global minimum distance from each parcel to its nearest sensory-motor landmarks for each participant (see Method 4.6 for detailed information). These four groups of parcels exhibited a decreasing distance from sensory-motor cortex: association-only parcels were furthest away, followed by association and non-semantic parcels, then feature and non-semantic parcels, and finally, feature-only parcels were the closest to sensory-motor cortex (association-only versus association and non-semantic: $t(244) = 118.32$, $p = 1.53 * e-217$; association and non-semantic versus feature and non-semantic: $t(244) = 51.94$, $p = 6.48 * e-134$; feature and non-semantic versus feature-only: $t(244) = 210.68$, $p = 5.18 * e-278$). All p-values are FDR-corrected. These findings show that the difficulty of semantic associations prompts a more anterior response in regions further from the sensory-motor cortex compared to feature matching.

Situating semantic control effects in a brain state space defined by the dimensions of intrinsic connectivity

The analyses above show that the difficulty effects in semantic association and feature matching tasks exhibit distinct topographical patterns. To reveal how these diverse control processes are organized on the cortical surface, we examined how neural patterns related to task difficulty were situated in a whole-brain state space. This space was defined by the top three dimensions of intrinsic connectivity, identified from resting-state functional MRI data of 245 participants in the S900 release of the HCP dataset, who completed four resting-state scans. Consistent with prior research[11,31,32], we focused on the first three connectivity dimensions, which showed the largest eigenvalues (as seen in Fig. 5d scree plot). The first dimension, explaining the most variance (12.75%), separated unimodal (purple-blue in Fig. 5a) from transmodal regions (red-white in Fig. 5a). The second dimension, accounting for 11.29% of the variance, separated somatomotor from auditory cortex (purple-blue in Fig. 5b) from visual cortex (red-white in Fig. 5b). The third dimension, explaining 3.98% of the variance, separated FPCN regions (purple-blue in Fig. 5c) from DMN regions (red-white in Fig. 5c).

To elucidate the relationship between task difficulty effects of semantic tasks and the three connectivity dimensions, we calculated their spatial correlation across all brain parcels. All p-values were computed using spin permutation, which accounts for spatial autocorrelation, and were FDR corrected to control for multiple comparison. In the semantic association task, the difficulty effect positively correlated with the first dimension in the left hemisphere; control of the retrieval of global associations fell towards the heteromodal end of this component (LH: $r = 0.32$, $p = 0.04$; RH: $r = 0.24$, $p = 0.09$). There was no significant correlation with the second dimension, indicating a balanced recruitment of auditory-motor and visual processes during controlled retrieval of global associations (LH: $r = 0.06$, $p = 0.39$; RH: $r = 0.02$, $p = 0.46$). There was no significant correlation with the third dimension, suggesting an equal recruitment of control and DMN networks (LH: $r = 0.04$, $p = 0.40$; RH: $r = 0.13$, $p = 0.16$).

In contrast, the difficulty effect in the feature matching task negatively correlated with the first dimension in the right hemisphere, indicating difficulty modulated activation more in sensory-motor areas than heteromodal areas (LH: $r = -0.24$, $p = 0.12$; RH: $r = -0.36$, $p = 0.03$). There was no correlation with the second dimension (LH: $r = 0.36$, $p = 0.08$; RH: $r = 0.36$, $p = 0.08$). However, a positive correlation was observed with the third dimension, showing stronger difficulty effects towards the control end than the DMN end (LH: $r = 0.46$, $p = 0$; RH: $r = -0.33$, $p = 0.005$).

Next, we compared the difficulty effects of the two semantic tasks within the brain state space. We calculated and transformed Pearson r correlations, which indicated the similarity between each connectivity dimension and the difficulty effect for each participant, to Fisher's z values. The first dimension (heteromodal-unimodal) showed a stronger correlation with the effect of difficulty in semantic association task than feature matching task ($t(27) = 3.921$, $p = 0.001$; Fig. 5g). This suggests that controlled retrieval in the association task involved heteromodal processes more strongly, whereas controlled retrieval in the feature matching task was more modality-specific. The second dimension (visual-motor) had a stronger correlation with the effect of difficulty in feature matching than in semantic association ($t(27) = -0.154$, $p = 0.019$; Fig. 5g), indicating that controlled responses in feature matching predominantly involved visual processing, while the association task showed a more balanced involvement of visual and motor information. Lastly, the third dimension (control-DMN) showed a greater correlation with the difficulty effect in feature matching than in association judgments ($t(27) = -4.162$, $p = 0$; Fig. 5g). This indicates that feature matching relied more on the functional separation between domain-general executive processes and the long-term memory functions of the DMN, whereas the semantic association task engaged these networks in a more integrated manner (cf. [11,25]).

Comparison of the locations of difficulty effects in state space for semantic and non-semantic tasks

To compare the locations of difficulty effects in state space for semantic and non-semantic tasks, we first calculated correlations between non-semantic difficulty effects and the three dimensions. Figures 6a and 6b show unthresholded difficulty effects for spatial working memory and math tasks, respectively. These spatial patterns correlated positively with the third dimension of intrinsic connectivity, which distinguishes control from DMN (spatial working memory - LH: $r = 0.56$, $p = 0$; RH: $r = 0.60$, $p = 0$; math tasks

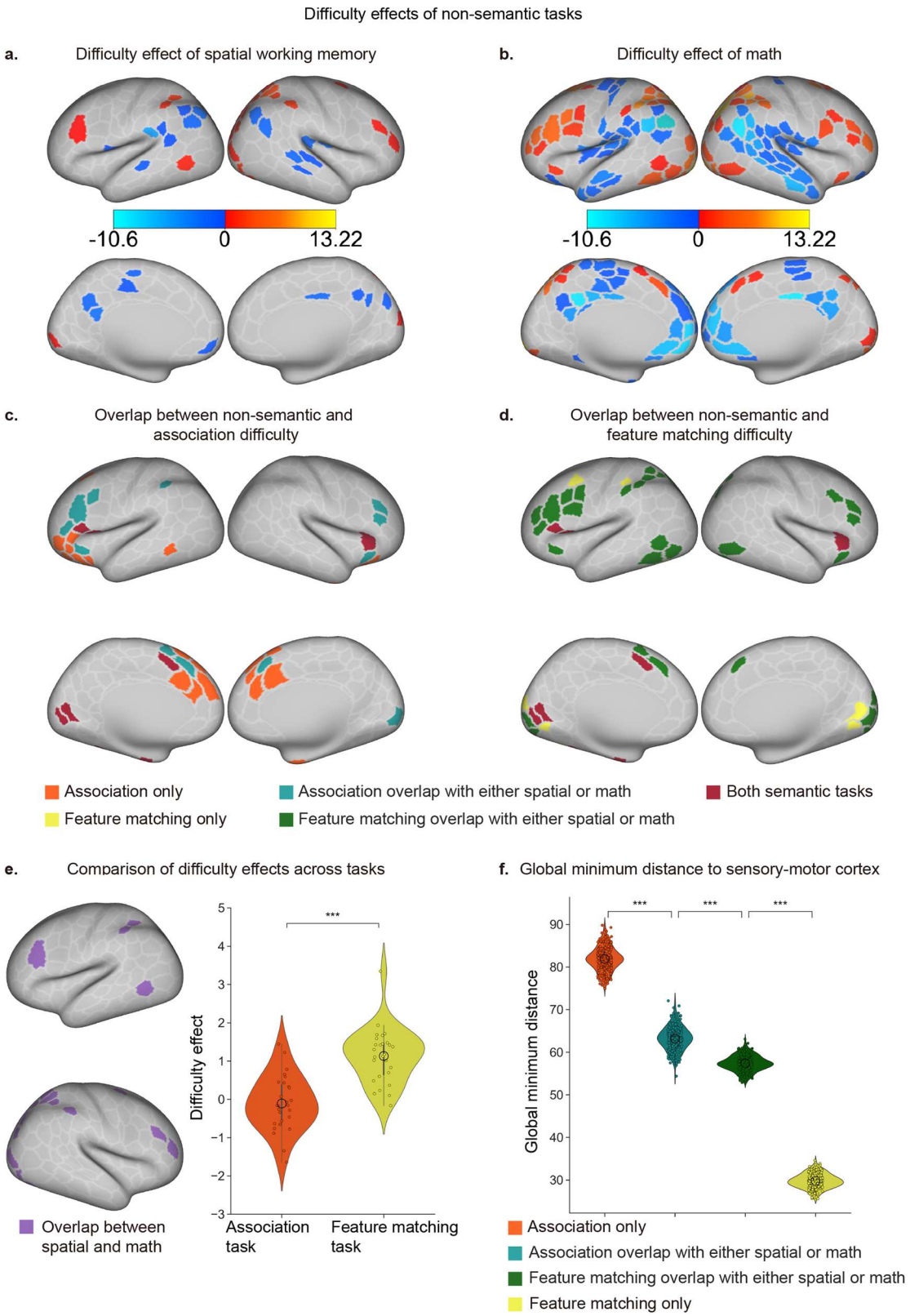

- LH: $r = 0.61$, $p = 0$; RH: $r = 0.63$, $p = 0$). There were no significant correlations with dimension 1 and 2 (uncorrected $p > 0.05$).

We then compared the correlations between connectivity dimensions and difficulty effects in the non-semantic tasks with the correlations between connectivity dimensions and difficulty effects in the semantic tasks. The first dimension of intrinsic connectivity was more associated with non-semantic difficulty than with task demands in the feature matching task (comparison for spatial working memory: t (26) = 2.26, $p = 0.04$; comparison for math: t (26) = 3.31, $p = 0.006$; Fig. 6c). There were no differences between non-semantic difficulty and task demands in semantic association (spatial working memory: t (26) = −1.96, $p = 0.07$; math: t (26) = −1.12, $p = 0.31$; Fig. 6c). These findings indicate that both semantic and non-semantic

Fig. 4 | Difficulty effects of spatial working memory and math tasks and their intersection with semantic tasks. a, **b** Difficulty effects in spatial working memory and math tasks, respectively. Warm colors indicate regions with increased activation during harder trials, while cold colors show regions with greater activation in easier trials ($p < 0.05$, FDR-corrected). **c** Overlap of regions with positive difficulty effects in the semantic association task (orange) and those responsive to non-semantic control demands (turquoise). **d** Overlap of regions with positive difficulty effects in the semantic feature matching task (yellow) and those responsive to non-semantic control demands (green). Red regions indicate difficulty effects present in both semantic tasks but not in the non-semantic tasks. **e** Greater difficulty effect in semantic feature matching compared to semantic association task within MDN regions (i.e., overlapping regions showing positive effects of difficulty in both spatial working memory and math tasks). **f** The global minimum distance to sensory-motor cortex for four types of parcels in **c** and **d**, each exhibiting a different pattern of difficulty across tasks. These groups of parcels showed a gradient in their distance from sensory-motor cortex: association-only parcels were the most distant, followed by association and non-semantic parcels, then feature and non-semantic parcels, with feature-only parcels being the closest. (***$p = 0.001$, FDR corrected).

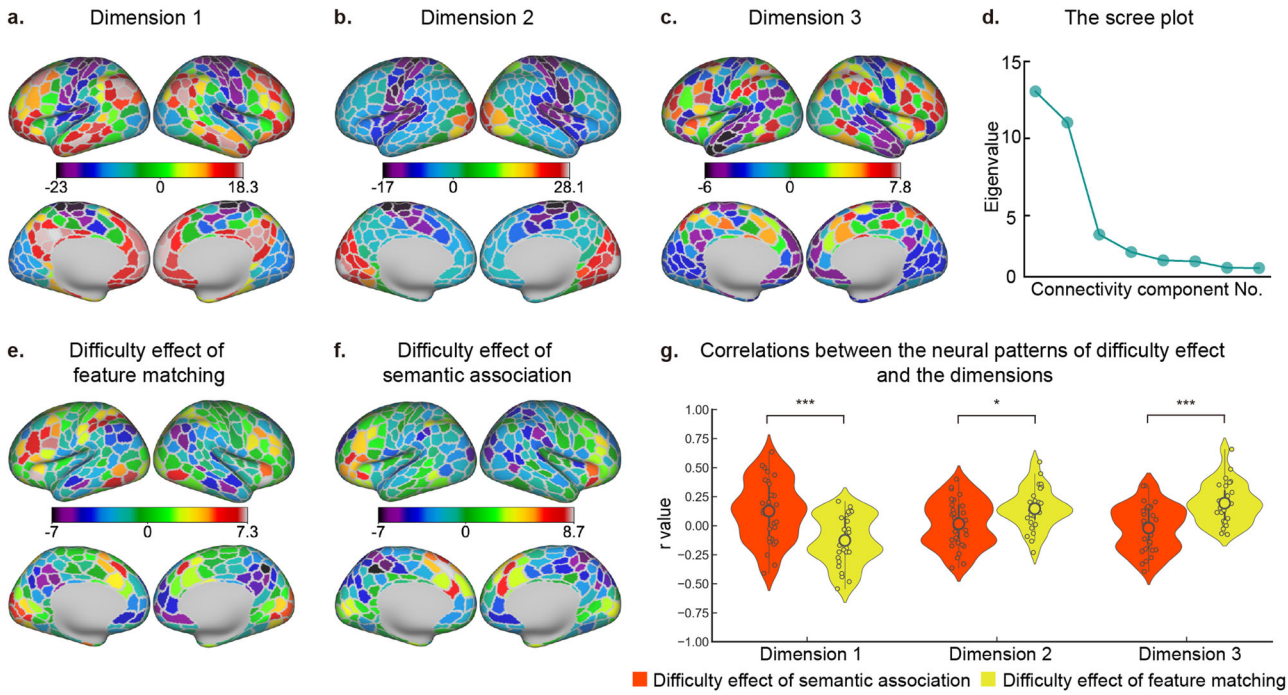

Fig. 5 | Spatial correspondence between effects of difficulty in semantic tasks and the top three dimensions of intrinsic connectivity. a–c The first three connectivity dimensions identified through decomposition of the whole brain FC matrix. The first dimension corresponds to the principal gradient that separates sensory-motor regions (purple-blue) from transmodal areas (red-white). The second dimension separates auditory-motor cortex (purple-blue) from visual cortex (red-white). The third dimension separates FPCN regions (purple-blue) from DMN regions (red-white). **d** The scree plot showing eigenvalue of each dimension. **e**, **f** Unthresholded maps of the effects of difficulty in the semantic association and semantic feature matching tasks. **g** Correlation between unthresholded effects of difficulty in each semantic task and the three connectivity dimensions. Effects of difficulty in the two semantic tasks dissociate within the brain space delineated by the dimensions of intrinsic connectivity, with effects of associative strength relating more to dimension 1, and effects of feature similarity relating more to dimension 3. (*$p = 0.05$; ***$p = 0.001$, FDR corrected).

difficulty effects can fall towards the heteromodal end of the first dimension; in contrast, the feature matching task that involved the goal-driven retrieval of visual features for words was less heteromodal.

The second dimension of intrinsic connectivity, distinguishing visual from auditory-motor processes, showed greater correlation with non-semantic difficulty than task demands in the association matching task (spatial working memory versus association: t (26) = 3.09, $p = 0.006$; math versus association: t (26) = 5.467, $p < 0.0001$; Fig. 6c). These results suggest that non-semantic tasks may involve more visual processing. Conversely, there was no significant difference between difficulty effects in spatial working memory and semantic feature matching (t (26) = 0.515, $p = 0.609$; Fig. 6c); however, difficulty effects in the math task showed a stronger positive correlation than task demands in feature matching (t (26) = 2.963, $p = 0.008$; Fig. 6c).

The third dimension of intrinsic connectivity, which separates control from DMN regions, correlated more strongly with difficulty effects in math compared with both semantic association (t (26) = 9.17, $p < 0.0001$; Fig. 6c) and feature matching tasks (t (26) = 4.48, $p < 0.0001$; Fig. 6c). Additionally, this dimension was more strongly correlated with spatial working memory than with task demands in semantic association (t (26) = 5.67, $p = 0$; Fig. 6c), but no significant difference was found for feature matching (t (26) = 0.86, $p = 0.39$; Fig. 6c). All the p-values were FDR corrected. These findings suggest that, on a dimension distinguishing control from DMN, difficulty effects in non-semantic tasks bear more similarity to those for feature matching than for global semantic associations.

Discussion

This study examines how cognitive control processes are organized on the cortical surface and within a brain state space defined by key dimensions of whole-brain intrinsic connectivity. We contrasted two semantic tasks—global association judgements and feature matching—and parametrically varied their difficulty by manipulating strength of association and feature similarity, to establish how brain networks are configured appropriately to control retrieval in these two contexts. We also compared controlled semantic cognition with the neural response to non-semantic control demands. We found that demanding semantic association trials elicited more activation in anterior portions of prefrontal and temporal cortex, while difficult semantic feature matching trials produced more posterior activation that overlapped to a greater extent with non-semantic multiple-demand regions. Differences were also found in whole-brain state space: the

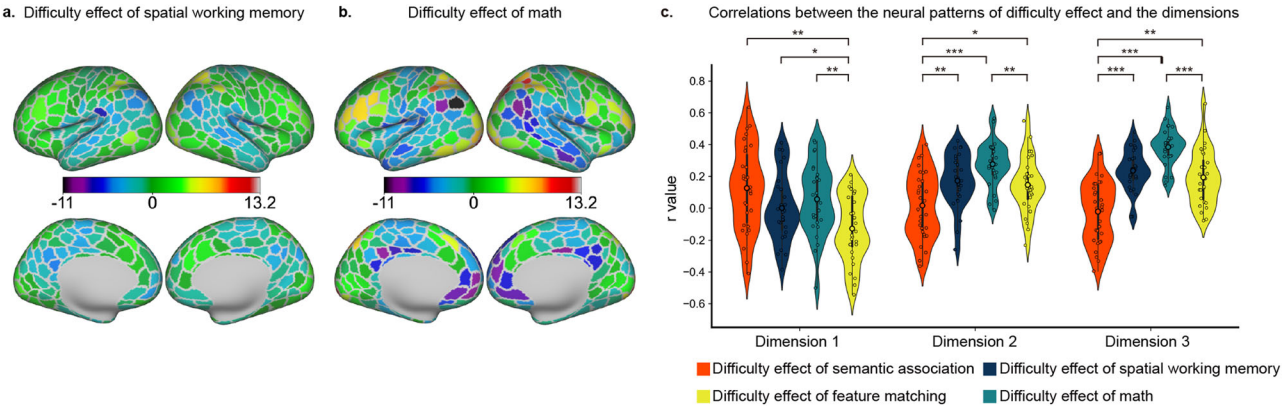

Fig. 6 | The spatial correspondence between effects of difficulty in non-semantic tasks and the dimensions of intrinsic connectivity. a, **b** Unthresholded maps of the effects of difficulty in the spatial working memory and math tasks. **c** The correlation between unthresholded effects of difficulty in each task and the three connectivity dimensions. Only the third dimension (control-DMN) correlated with the effects of difficulty in the two non-semantic tasks. The non-semantic tasks were also more similar to the feature matching than the association task on this dimension. (*$p = 0.05$; **$p = 0.01$; ***$p = 0.001$, FDR corrected).

difficulty effects in global semantic associations were closer to the heteromodal end of a heteromodal-unimodal dimension than those in feature matching. Additionally, the association task demonstrated balanced recruitment between visual and auditory-motor representations on the second dimension and engaged both executive and DMN regions on the third dimension. In contrast, difficulty effects in semantic feature matching more closely resembled non-semantic task demands on the second and third dimensions, indicating greater visual and executive responses with less DMN involvement. These results collectively suggest there are at least two distinct large-scale brain states supporting controlled semantic cognition: one state is more heteromodal and involves more equal recruitment of control and DMN regions, while the other state is visually focused and engages control regions more selectively without concurrent DMN activation. Furthermore, these aspects control are underpinned by distinct dimensions of functional variation within whole-brain state space.

Semantic knowledge is multifaceted, drawing on support from diverse brain regions[1]. In our two semantic tasks, we utilized identical stimuli and presented them in the same format. Thus, the primary distinction between these tasks lies in the nature of the controlled retrieval process. The feature matching task predominantly relies on the controlled retrieval of visual features, while the semantic association task requires participants to draw upon heteromodal information since understanding the inherent relationships between word pairs involves integrating knowledge across various sensory experiences and modalities[14–16]. We show that the configuration of control processes that support cognition in a neural state space can reflect the type of information that participants are required to focus on, rather than simply the use of verbal materials, or the superficial characteristics of the task.

Recent research demonstrates that control regions modulate their activity and interaction patterns in a context-specific manner to support adaptable behavior across domains[33,34]. These regions dynamically modify their baseline communication to integrate more specialized brain areas, facilitating task-specific[35–37]. In neural state-space analysis, we found that this flexibility might relate to different network configurations underpinned by distinct dimensions of intrinsic connectivity. Specifically, control regions are proximal to DMN regions on the first dimension but are separated from DMN regions on the third dimension. This allows for whole-brain states in which heteromodal memory and control regions are either integrated (supporting task demands in association judgments) or segregated (supporting task demands in feature matching). These findings align with previous research suggesting that SCN and MDN are dissociable control networks: SCN appears to relate to the first neural dimension in which heteromodal memory and control networks are functionally coupled, while non-semantic controlled states linked to strong activation within MDN elicit anti-correlation between control and DMN regions, as captured by the third dimension[7,8,11,38]. In line with this proposal, regions of LIFG associated with maintaining and applying a semantic goal to constrain retrieval in a top-down fashion showed negative connectivity with DMN, while LIFG regions associated with the controlled retrieval of weak associations showed positive connectivity to some DMN regions[39]. Neural state space analysis provides an account of both the commonalities and distinctions among various controlled states and explains why SCN and MDN are adjacent, yet topographically distinct.

Tasks involving global associations draw on diverse sensory-motor information, and therefore brain states that selectively focus on one modality are not conducive to the task. Here, control regions need to interact with heteromodal semantic knowledge to identify conceptual links between weakly related concepts and, consequently, heteromodal control and semantic memory networks are thought to be coupled in these circumstances[25]. Consistent with this, control networks and DMN can show similar representational content[30,40] and both networks are modulated by prior knowledge[40,41]. Conversely, tasks like visual feature matching demand a brain state in which visual (rather than auditory-motor) features dominate cognition. As decision-making hinges on one specific feature, control regions supporting goal maintenance and the prioritization of relevant knowledge need to be functionally separated from heteromodal conceptual knowledge and more tightly integrated with brain regions representing task-relevant information[42].

The concept of brain states offers a promising framework to understand neural flexibility and cognitive control, yet our study has limitations. Firstly, we focused on a neural state space defined by the top three dimensions of intrinsic connectivity, given these components explain the most variance and have clear interpretations in terms of functional relationships within and between heteromodal and unimodal cortex that are highly relevant to our task manipulations. However, cognitive control might be related to more than just these three dimensions. A more comprehensive understanding of the varieties of cognitive control will require exploring higher-dimensional state spaces. Secondly, although our tasks effectively demonstrate that distinct aspects of semantic control are related to different dimensions of brain state space, cognitive control can be modulated in numerous ways. Future research employing a broader array of tasks is essential to examine whether there are two primary dimensions of controlled behavior, one stabilized by heteromodal long-term memory and the other by control processes independent of memory. For example, it would be useful to test this claim by extending our approach of manipulating task demands parametrically to non-semantic control tasks within the same participants. Despite these constraints, our study demonstrates that at least

two neural dimensions are crucial to encompass the diverse range of controlled processes we employ to tailor cognition to the context.

Methods

Participants

All participants were right-handed, native English speakers, with normal or corrected-to-normal vision and no history of psychiatric or neurological illness. All participants provided informed consent. For the University of York datasets, the research was approved by the York Neuroimaging Centre and Department of Psychology ethics committees. For the HCP dataset, the study was approved by the Institutional Review Board of Washington University at St. Louis[43]. All ethical regulations relevant to human research participants were followed.

31 healthy adults performed the semantic tasks (25 females; age: mean ± SD = 21.26 ± 2.93, range: 19–34 years). A functional run was excluded if (I) relative root mean square (RMS) framewise displacement was higher than 0.2 mm, (II) more than 15% of frames showed motion exceeding 0.25 mm, or (III) the accuracy of the behaviour task was low (3 SD below the mean). If only one run of a task was left for a participant after exclusion, all their data for that task were removed. Using the exclusion criteria above for the feature matching task, there were 23 participants with 4 runs, 4 participants with 3 runs, and 1 participant with 2 runs. For the association task, there were 24 participants with 4 runs, 3 participants with 3 runs, and 3 participants with 2 runs. An additional 30 native English speakers, who did not take part in the main fMRI experiment, rated the color and shape similarity and semantic association strength for each word pair (21 females; age range: 18–24 years).

31 healthy adults (26 females; age: mean ± SD = 20.60 ± 1.68, range: 18–25 years) performed the spatial working memory and math tasks. One participant with incomplete data was removed. These exclusion criteria above resulted in a final sample of 27 participants for both the spatial working memory task and the math task.

The HCP sample involved data from 245 healthy volunteers (115 females; age: mean ± SD = 28.21 ± 3.67, range: 23–35 years)[43].

Task paradigms

Semantic association task. Participants made yes/no decisions to pairs of words to indicate if they were semantically associated in general or not. Overall, there were roughly equal numbers of 'related' and 'unrelated' responses across participants. For example, DALMATIAN and COW are semantically related; COAL and TOOTH are not. Similarly, we parametrically manipulated the semantic association strength between the probe and target concepts, using semantic association strength ratings taken from a separate group of 30 participants on a 5-point Likert Scale. For example, in related trials, the association strength between PUMA and LION is very strong (i.e., 4.8) while for TIGER and WHALE is relatively weak (i.e., 4.0; although they are still both animals and are semantically related). In non-related trials, the association strength between KINGFISHER and SCORPION is relatively high (i.e., 2.1) while BANANA and BRICK is very low (i.e., 1.0) although participants thought neither were related. For the related trials, stronger associations would facilitate decision making, while for unrelated trials, stronger associations interfere with the decision making. This parametric design allowed us to model the effect of decision difficulty and test whether how this is related to dimensions of brain organization.

This task included four runs, presented in a rapid event-related design. Each run consisted of 80 trials, with about half being related and half being unrelated trials. The procedure was the same as the feature matching task except only two words were presented on the screen. The feature and association tasks were separated by one week.

Semantic feature matching task. Participants made yes/no decisions about whether probe and target concepts (presented as words) were matched in terms of a particular semantic feature (colour or shape), specified at the top of the screen during each trial. The feature prompt, probe word, and target words were presented simultaneously. Half of the trials were matching trials in which participants were expected to identify shared features; while half of the trials were non-matching trials in which participants would not be expected to identify shared features. For example, in a colour matching trial, participants would answer 'yes' to the word-pair DALMATIAN – COW, due to their colour similarity, whereas they would answer 'no' to COAL – TOOTH as they do not share a similar colour. The same stimuli were used in the semantic feature matching task and semantic association task.

We parametrically manipulated the degree of feature similarity between the probe and target concepts, using semantic feature similarity ratings taken from a separate group of 30 participants on a 5-point Likert Scale. For instance, in colour-matching trials, the degree of colour similarity between DALMATIAN and COW was found to be very high (i.e., 4.8), while that between PUMA and LION was relatively low (i.e., 4.0), despite that participants believe that the two trials had similar colour. Conversely, in colour non-matching trials, the degree of colour similarity between CROW and HUMMINGBIRD was relatively high (i.e., 2.5), whereas that between COAL and TOOTH was very low (i.e., 1.0), even though the participants perceived no similarity in colour. Greater feature similarity facilitates the decision-making process for the matching trials but makes the decision more difficult for the non-matching trials. This parametric design allowed us to model the effect of the decision difficulty during the controlled retrieval of visual features in the neural data, and test how it is related to dimensions of brain organization.

This task included four runs and two conditions (two features: colour and shape), presented in a mixed design. Each run consisted of four experimental blocks (two 2 min 30 s blocks per feature), resulting in a total time of 10 min 12 s. In each block, 20 trials were presented in a rapid event-related design. To maximize the statistical power of the rapid event-related fMRI data analysis, the stimuli were presented with a temporal jitter randomized from trial to trial[44]. The inter-trial interval varied from 3 to 5 s. Each trial started with a fixation, followed by the feature, probe word, and target word presented centrally on the screen, triggering the onset of the decision-making period. The feature, probe word, and target word remained visible until the participant responded, or for a maximum of 3 s. The condition order was counterbalanced across runs and run order was counterbalanced across participants. Half of the participants pressed a button with their right index finger to indicate a matching trial and responded with their right middle finger to indicate a non-matching trial. Half of the participants pressed the opposite buttons.

Spatial working memory task. Participants were required to maintain four or eight sequentially presented locations in a 3 × 4 grid[45], giving rise to easy and hard spatial working memory conditions. Stimuli were presented at the center of the screen across four steps. Each of these steps lasted for 1 s and highlighted one location on the grid in the easy condition, and two locations in the hard condition. This was followed by a decision phase, which showed two grids side by side (i.e., two-alternative forced choice paradigm). One grid contained the locations shown on the previous four steps, while the other contained one or two locations in the wrong place. Participants indicated their response via a button press and feedback was immediately provided within in 2.5 s. Each run consisted of 12 experimental blocks (6 blocks per condition and 4 trials in a 32 s block) and 4 fixation blocks (each 16 s long), resulting in a total time of 448 s.

Math task. Participants were presented with an addition expression on the screen for 1.45 s and, subsequently made a two-alternative forced choice decision indicating their solution within 1 s. The easy condition used single-digit numbers while the hard condition used two-digit numbers. Each trial ended with a blank screen lasting for 0.1 s. Each run consisted of 12 experimental blocks (with 4 trials per block) and 4 fixation blocks, resulting in a total time of 316 s.

Image acquisition

Image acquisition of York Semantic dataset. Whole brain structural and functional MRI data were acquired using a 3 T Siemens MRI scanner utilising a 64-channel head coil, tuned to 123 MHz at York Neuroimaging Centre, University of York. The functional runs were acquired using a multi-band multi-echo (MBME) EPI sequence, each 11.45 minutes long (TR = 1.5 s; TE = 12, 24.83, 37.66 ms; 48 interleaved slices per volume with slice thickness of 3 mm (no slice gap); FoV = 24 cm (resolution matrix = 3 × 3 × 3; 80 × 80); 75° flip angle; 455 volumes per run; 7/8 partial Fourier encoding and GRAPPA (acceleration factor = 3, 36 ref. lines); multi-band acceleration factor = 2). Structural T1-weighted images were acquired using an MPRAGE sequence (TR = 2.3 s, TE = 2.3 s; voxel size = 1 × 1 × 1 isotropic; 176 slices; flip angle = 8°; FoV= 256 mm; interleaved slice ordering). We also collected a high-resolution T2-weighted (T2w) scan using an echo-planar imaging sequence (TR = 3.2 s, TE = 56 ms, flip angle = 120°; 176 slices, voxel size = 1 × 1 × 1 isotropic; Fov = 256 mm).

Image acquisition of York Non-semantic dataset. MRI acquisition protocols have been described previously[11,30]. Structural and functional data were collected on a Siemens Prisma 3 T MRI scanner at the York Neuroimaging Centre. The scanning protocols included a T1-weighted MPRAGE sequence with whole-brain coverage. The structural scan used: acquisition matrix of 176 × 256 × 256 and voxel size 1 × 1 × 1 mm^3, repetition time (TR) = 2300 ms, and echo time (TE) = 2.26 ms. Functional data were acquired using an EPI sequence with an 800 flip angle and using GRAPPA with an acceleration factor of 2 in 3 × 3 × 4 mm voxels in 64-axial slices. The functional scan used: 55 3-mm-thick slices acquired in an interleaved order (with 33% distance factor), TR = 3000 ms, TE = 15 ms, FoV = 192 mm.

Image acquisition of HCP dataset. MRI acquisition protocols of the HCP dataset have been previously described[43,46]. Images were acquired using a customized 3 T Siemens Connectome scanner having a 100 mT/m SC72 gradient set and using a standard Siemens 32-channel radio-frequency receive head coil. Participants underwent the following scans: structural (at least one T1-weighted (T1w) MPRAGE and one 3D T2-weighted (T2w) SPACE scan at 0.7-mm isotropic resolution), rsfMRI (4 runs × 14 min and 33 s), and task fMRI (7 tasks, 46.6 min in total). Since not all participants completed all scans, we only included 339 unrelated participants from the S900 release. Whole-brain rsfMRI and task fMRI data were acquired using identical multi-band echo planar imaging (EPI) sequence parameters of 2-mm isotropic resolution with a TR = 720 ms. Spin echo phase reversed images were acquired during the fMRI scanning sessions to enable accurate cross-modal registrations of the T2w and fMRI images to the T1w image in each subject and standard dual gradient echo field maps were acquired to correct T1w and T2w images for readout distortion. Additionally, the spin echo field maps acquired during the fMRI session (with matched geometry and echo spacing to the gradient echo fMRI data) were used to compute a more accurate fMRI bias field correction and to segment regions of gradient echo signal loss.

Subjects were considered for data exclusion based on the mean and mean absolute deviation of the relative root-mean-square motion across four rsfMRI scans, resulting in four summary motion measures. If a subject exceeded 1.5 times the interquartile range (in the adverse direction) of the measurement distribution in two or more of these measures, the subject was excluded. In addition, functional runs were flagged for exclusion if more than 25% of frames exceeded 0.2 mm frame-wise displacement (FD_power). These above exclusion criteria were established before performing the analysis[47,48]. The data of 91 participants was excluded because of excessive head motion and the data of another 3 participants was excluded because their resting data did not have all the time points. In total, the data of 245 participants was analysed after exclusions.

Image pre-processing

Image pre-processing of York Semantic and Non-semantic dataset. The York datasets were preprocessed using fMRIPrep 20.2.1 [49, RRID:SCR_016216], which is based on Nipype 1.5.1 [50, RRID:SCR_002502].

Anatomical data preprocessing. The T1w image was corrected for intensity non-uniformity (INU) with N4BiasFieldCorrection[51], distributed with ANTs 2.3.3 [52, RRID:SCR_004757], and used as T1w-reference throughout the workflow. The T1w-reference was then skull-stripped with a Nipype implementation of the antsBrainExtraction.sh workflow (from ANTs), using OASIS30ANTs as target template. Brain tissue segmentation of cerebrospinal fluid (CSF), white-matter (WM) and gray-matter (GM) was performed on the brain-extracted T1w using fast FSL 5.0.9 [53, RRID:SCR_002823]. Brain surfaces were reconstructed using recon-all from FreeSurfer 6.0.1 [54, RRID:SCR_001847], and the brain mask estimated previously was refined with a custom variation of the method to reconcile ANTs-derived and FreeSurfer-derived segmentations of the cortical gray-matter of Mindboggle [55, RRID:SCR_002438]. Volume-based spatial normalization to two standard spaces (MNI152NLin2009cAsym, MNI152NLin6Asym) was performed through nonlinear registration with antsRegistration (ANTs 2.3.3), using brain-extracted versions of both T1w reference and the T1w template. The following templates were selected for spatial normalization: ICBM 152 Nonlinear Asymmetrical template version 2009c [56, RRID:SCR_008796; TemplateFlow ID: MNI152NLin2009cAsym], FSL's MNI ICBM 152 non-linear 6th Generation Asymmetric Average Brain Stereotaxic Registration Model [57, RRID:SCR_002823; TemplateFlow ID: MNI152NLin6Asym].

Functional data preprocessing. For each of the BOLD runs per subject, the following preprocessing was performed. First, a reference volume and its skull-stripped version were generated using a custom methodology of fMRIPrep. A B0-nonuniformity map (or fieldmap) was estimated based on a phase-difference map calculated with a dual-echo GRE (gradient-recall echo) sequence, processed with a custom workflow of SDCFlows inspired by the epidewarp.fsl script and further improvements in HCP Pipelines[43]. The fieldmap was then co-registered to the target EPI reference run and converted to a displacements field map (amenable to registration tools such as ANTs) with FSL's fugue and other SDCflows tools. Based on the estimated susceptibility distortion, a corrected EPI reference was calculated for a more accurate co-registration with the anatomical reference. The BOLD reference was then co-registered to the T1w reference using bbregister (FreeSurfer) which implements boundary-based registration[58]. Co-registration was configured with six degrees of freedom. Head-motion parameters with respect to the BOLD reference (transformation matrices, and six corresponding rotation and translation parameters) were estimated before any spatiotemporal filtering using mcflirt (FSL 5.0.9[59]). BOLD runs were slice-time corrected using 3dTshift from AFNI 20160207 [60, RRID:SCR_005927]. The BOLD time-series were resampled onto the following surfaces (FreeSurfer reconstruction nomenclature): fsaverage. Grayordinates files[43] containing 91k samples were also generated using the highest-resolution fsaverage as intermediate standardized surface space. Several confounding time-series were calculated based on the preprocessed BOLD: framewise displacement (FD), DVARS (D refers to a derivative of fMRI time course, VARS refers to RMS variance) and three region-wise global signals. FD was computed using two formulations following previous work (absolute sum of relative motion;[61], relative root mean square displacement between affines;[59]. FD and DVARS were calculated for each functional run, both using their implementations in Nipype[61]. Three global signals were extracted within the CSF, the WM, and the whole-brain masks. Additionally, a set of physiological regressors were extracted to allow for component-based noise correction (CompCor)[62] principal components were estimated after high-pass filtering the preprocessed

BOLD time-series (using a discrete cosine filter with 128 s cut-off) for two CompCor variants: temporal (tCompCor) and anatomical (aCompCor). tCompCor components were then calculated from the top 2% variable voxels within the brain mask. For aCompCor, three probabilistic masks (CSF, WM and combined CSF + WM) were generated in anatomical space. The implementation differs from that of Behzadi et al. [62] in that instead of eroding the masks by 2 pixels in BOLD space, the aCompCor masks are subtracted from a mask of pixels that likely contain a volume fraction of GM. This mask is obtained by dilating a GM mask extracted from the FreeSurfer's aseg segmentation, and it ensures components are not extracted from voxels containing a minimal fraction of GM. Finally, these masks are resampled into BOLD space and binarized by thresholding at 0.99 (as in the original implementation). Components were also calculated separately within the WM and CSF masks. For each CompCor decomposition, the k components with the largest singular values were retained, such that the retained components' time series were sufficient to explain 50 percent of variance across the nuisance mask (CSF, WM, combined, or temporal). The remaining components were dropped from consideration. The head-motion estimates calculated in the correction step were also placed within the corresponding confounds file. The confound time series derived from head motion estimates and global signals were expanded with the inclusion of temporal derivatives and quadratic terms for each[63]. Frames that exceeded a threshold of 0.5 mm FD or 1.5 standardized DVARS were annotated as motion outliers. All resamplings were performed with a single interpolation step by composing all the pertinent transformations (i.e., head-motion transform matrices, susceptibility distortion correction when available, and co-registrations to anatomical and output spaces). Gridded (volumetric) resamplings were performed using antsApplyTransforms (ANTs), configured with Lanczos interpolation to minimize the smoothing effects of other kernels[64]. Non-gridded (surface) resamplings were performed using mri_vol2surf (FreeSurfer). fMRIPrep used Nilearn 0.6.2 [65, RRID:SCR_001362], mostly within the functional processing workflow. The resulting data were in CIFTI 64k-vertex grayordinate space. The left hemisphere had 29696 vertices and right hemisphere had 29716 vertices in total after removing the medial wall.

Post-processing of the outputs of fMRIPrep version 20.2.1[49] was performed using the eXtensible Connectivity Pipeline (XCP)[63,66]. For each CIFTI run per subject, the following post-processing was performed: before nuisance regression and filtering any volumes with framewise-displacement greater than 0.3 mm[61,63] were flagged as outliers and excluded from nuisance regression. In total, 36 nuisance regressors were selected from the nuisance confound matrices of fMRIPrep output. These nuisance regressors included six motion parameters, global signal, mean white matter, and mean CSF signal with their temporal derivatives, and the quadratic expansion of six motion parameters, tissue signals and their temporal derivatives[63,66]. These nuisance variables were accounted for in the BOLD data using linear regression—as implemented in Scikit-Learn 0.24.2[67]. Residual timeseries from this regression were then band-pass filtered to retain signals within the 0.01–0.08 Hz frequency band. The processed BOLD was smoothed using Connectome Workbench with a gaussian kernel size of 6.0 mm (FWHM). Processed functional timeseries were extracted from residual BOLD using Connectome Workbench[43] for the Kong atlas[68]. Many internal operations of XCP use Nibabel[65], numpy[69], and scipy[69].

Image pre-processing of HCP dataset. We used HCP's minimal preprocessing pipelines[43]. Briefly, for each subject, structural images (T1w and T2w) were corrected for spatial distortions. FreeSurfer v5.3 was used for accurate extraction of cortical surfaces and segmentation of subcortical structures[70,71]. To align subcortical structures across subjects, structural images were registered using non-linear volume registration to the Montreal Neurological Institute (MNI152) space. Functional images (rest and task) were corrected for spatial distortions, head motion, and mapped from volume to surface space using ribbon-constrained volume to surface mapping.

Subcortical data were also projected to the set of extracted subcortical structure voxels and combined with the surface data to form the standard CIFTI grayordinate space. Data were smoothed by a 2-mm FWHM kernel in the grayordinates space that avoids mixing data across gyral banks for surface data and avoids mixing areal borders for subcortical data. Rest and task fMRI data were additionally identically cleaned for spatially specific noise using spatial ICA + FIX[72] and global structured noise using temporal ICA[73]. For accurate cross-subject registration of cortical surfaces, a multimodal surface matching (MSM) algorithm[74] was used to optimize the alignment of cortical areas based on features from different modalities. MSMSulc ("sulc": cortical folds average convexity) was used to initialize MSMAll, which then utilized myelin, resting-state network, and rfMRI visuotopic maps.

Task fMRI analysis

Individual-specific parcellation. Considering the anatomical and functional variability across individuals[75–78], we estimated individual-specific areal-level parcellation using a multi-session hierarchical Bayesian model (MS-HBM)[68,79]. To estimate individual-specific parcellation, we acquired "pseudo-resting state" timeseries in which the task activation model was regressed from feature matching and semantic association fMRI data[80] using xcp_d (https://github.com/PennLINC/xcp_d). The task activation model and nuisance matrix were regressed out using AFNI's3dTproject (for similar implementation, see ref. 81).

Using a group atlas, this method calculates inter-subject resting-state functional connectivity variability, intra-subject resting-state functional connectivity variability, and finally parcellates for each single subject based on this prior information. As in Kong et al. [68,79], we used MS-HBM to define 400 individualized parcels belonging to 17 discrete individualized networks for each participant. Specifically, we calculated all participants' connectivity profiles, created the group parcellation using the average connectivity profile of all participants, estimated the inter-subject and intra-subject connectivity variability, and finally calculated each participant's individualized parcellation. This parcellation imposed the Markov random filed (MRF) spatial prior. We used a well-known areal-level parcellation approach, i.e., the local gradient approach (gMS-HBM), which detects local abrupt changes (i.e., gradients) in resting-state functional connectivity across the cortex[82]. A previous study[83] has suggested combining local gradient[82,84] and global clustering[85] approaches for estimating areal-level parcellations. Therefore, we complemented the spatial contiguity prior in contiguous MS-HBM (cMS-HBM) with a prior based on local gradients in resting-state functional connectivity, which encouraged adjacent brain locations with gentle changes in functional connectivity to be grouped into the same parcel. We used the pair of parameters (i.e., beta value = 50, w = 30 and c = 30), which was optimized using our own dataset. The same parameters were also used in Kong et al.[68]. Vertices were parcellated into 400 cortical regions (200 per hemisphere). To parcellate each of these parcels, we calculated the average time series of enclosed vertices to get better signal noise ratio (SNR) using Connectome Workbench software. This parcel-based time series was used for all the following analyses. The same method and parameters were used to generate the individual-specific parcellation for the participants in the HCP dataset using the resting-state time series except that the task regression was not performed.

Homogeneity of parcels. To evaluate whether a functional parcellation is successful, parcel homogeneity is commonly used[68,79,84]. Parcel homogeneity was calculated as the average Pearson's correlations between fMRI time courses of all pairs of vertices within each parcel, adjusted for parcel size and summed across parcels[68,79,83]. Higher homogeneity means that vertices within the same parcel share more similar time courses and indicates better parcellation quality. To summarize the parcel homogeneity, we averaged the homogeneity value across parcels. We calculated the parcel homogeneity for each run of each participant for each task using the individual-specific parcellation and then averaged them across runs for each participant for each task. We also

calculated the parcel homogeneity using canonical Yeo 17-network group atlas. Using the resting state data of the HCP dataset, Kong et al.[68] demonstrated that homogeneity within MS-HBM-based individualized parcels was greater than that in the canonical Yeo 17-network group atlas that does not consider variation in functional neuroanatomy. A similar pattern was observed using the York Semantic datasets[19].

Task fMRI univariate analysis. To reveal how the neural data were modulated by the difficulty of making decisions about global semantic associations and visual features, respectively, we conducted univariate analysis for the association task and feature matching task, respectively and then compared them. To examine parametric effects of task difficulty, we modelled the parametric effect of associative strength or feature similarity, including a parametric regressor for correct trials in the general linear model (GLM). Additionally, we included one task mean regressor to reveal the main effect of task, which is analogous to the inclusion of an intercept term in a linear regression model along with the slope term. The task mean effect was used to reveal the regions that showed greater or less activation during the tasks relative to the rest by extracting the beta value of each parcel in these task conditions and testing whether they were significantly activated (i.e., above zero) or deactivated (i.e., below zero) relative to implicit baseline (i.e., fixation period). For all the tasks, we also modelled incorrect trials as regressors of no interest. Demeaned semantic ratings and the main effect of task were modelled as epochs lasting from the trial onset to response, thus controlling for lengthened BOLD responses on trials with longer response times. Fixed-effects analyses were conducted using nilearn[65] to estimate the average effects across runs within each subject for each parcel. Then we conducted one-sample *t*-tests to assess whether the estimated effect-size (i.e., contrast) was significantly different from zero across all subjects. We conducted FDR correction at $p = 0.05$ to control for multiple comparisons. Finally, we identified the network that each parcel belonged to[68].

Then, we examined the difficulty effect for each task. We pinpointed brain regions that exhibited a stronger response to more difficult trials in the two semantic tasks. This increase in activation occurred when (i) association strength was lower for related 'Yes' trials or higher for unrelated 'No' trials in the semantic association task, and (ii) feature similarity was lower for matching 'Yes' trials or higher for non-matching 'No' trials in the feature matching task.

In the semantic association task, we modeled the parametric effect of difficulty using demeaned semantic association strength ratings. Our analysis focused on how neural responses varied with association strength: they were negatively modulated by association strength in related trials and positively modulated in non-related trials. Additionally, we identified brain regions that exhibited increased activation during easier trials, characterized by comparatively weak associative strength in associated trials and strong associative strength in non-associated trials.

Similarly, we examined the difficulty effect for the semantic feature matching task. We modeled the difficulty effect using demeaned feature similarity ratings. We examined how neural responses were modulated by these ratings: they were negatively modulated by feature similarity in matching trials and positively in non-matching trials. To identify specific brain regions involved, we extracted the beta values for each parcel. This helped reveal regions that demonstrated greater activation when feature similarity was lower in matching trials and higher in non-matching trials. Additionally, we identified regions that showed the opposite pattern, exhibiting greater deactivation in easier trials (i.e., when feature similarity was lower in matching trials and higher in non-matching trials). To directly compare differences in the activation patterns for the association judgment and feature matching tasks, we extracted the beta values relating to semantic difficulty for each parcel and each participant in each task and conducted paired *t*-tests.

We also examined regions where the neural responses were modulated by task difficulty in spatial working memory and math tasks. We included two regressors—hard and easy conditions to reveal regions showing greater activation in the hard than easy conditions. These parcels were thought to support domain-general executive control. We also modelled incorrect trials as regressors of no interest.

Comparison of semantic and non-semantic task demands. After determining the difficulty effects of both semantic and non-semantic tasks, we analyzed the extent of overlap between these effects in semantic tasks and brain regions responsive to non-semantic task demands through three complementary analyses. Firstly, we quantified the overlap in regions showing greater activation in semantic association task with those in either spatial working memory or math tasks. We also quantified such overlap for the semantic feature matching task. Secondly, we identified MDN regions by locating areas with difficulty effects in both spatial working memory and math tasks. We then compared the activation strength linked to task difficulty in these MDN regions for both semantic association and feature matching tasks. Lastly, we calculated and compared spatial correlations between the unthresholded maps of difficulty effects in non-semantic and semantic tasks. These analyses enabled us to investigate if the difficulty effect in the feature matching task showed a greater overlap with non-semantic control areas compared to the semantic association task. All *p*-values were FDR-corrected following spin permutation.

Given the spatial autocorrelation present in the task difficulty maps, we created a null distribution using spin permutation implemented in BrainSMASH[86]. This approach simulates brain maps, constrained by empirical data, that preserve the spatial autocorrelation of cortical parcellated brain maps. We subsequently compared the observed correlation values with the null distribution to determine whether the real correlations were significantly greater than that expected by spatial autocorrelation alone. This analysis was performed for the two hemispheres separately because the geodesic distance between parcels was used to generate the spatial-autocorrelation-preserving surrogate maps when creating the null distribution, and we could only measure geodesic distance between parcels within a hemisphere, because the left and right hemisphere surface maps were not on the same mesh.

The dimensions of intrinsic connectivity. We identified key dimensions of FC by performing dimension reduction analysis on resting state FC from the HCP dataset. First, we calculated the resting-state functional connectivity for each run of each participant by demeaning the residual time series for each parcel and then calculating the Pearson correlations for each parcel pair. We then averaged these individual connectivity matrices to generate a group-averaged connectivity matrix. We used the Brainspace Toolbox[87] to extract ten group-level gradients from the group-averaged connectivity matrix (dimension reduction technique = diffusion embedding, kernel = None, sparsity = 0.9), following the methodology of previous studies[31]. This analysis resulted in ten group-level gradients explaining maximal whole-brain connectivity variance in descending order. We retained the first few components explaining the most variance by looking at the eigenvalues of each component in the scree plots shown in Fig. 5D. The first three components, which explained 28.02% variance, had the largest eigenvalues, indicating their greater importance (see Fig. 5D for scree plot)

Correlation between parametric difficulty effects and connectivity components. We investigated whether the primary dimensions of brain organization, as captured by connectivity components, correspond to the topographical organization of the parametric effects of task difficulty. The semantic association task may rely more on the separation between sensory-motor and transmodal regions, essential for the controlled retrieval of long-term memory. Conversely, the feature matching task may rely more on the separation between domain-general control network and DMN, due to its goal maintenance demands that typically engage control networks that are anti-correlated with DMN. We examined the relationship between task difficulty effects, indicated by

parametric regressors, and functional organization dimensions, revealed through intrinsic connectivity components. This involved computing Pearson r correlations between the first three connectivity dimensions and difficulty effects of semantic and non-semantic tasks at the group level. Given the spatial autocorrelation present in both the principal connectivity gradient and task difficulty maps, we created a null distribution using spin permutation implemented in BrainSMASH[86].

To compare the locations of difficulty effects in state space for semantic and non-semantic tasks, we also calculated the Pearson r correlation between the first three connectivity components and the difficulty effect for each task for each participant and then converted the Pearson r values to Fisher z values. Finally, we compared the correlations for each task pair by conducting paired t test. We conducted FDR correction at $p = 0.05$ to control for multiple comparisons.

Structural MRI analysis

Cortical geometry—global minimum distance to primary sensory-motor landmarks. We investigated whether the demanding semantic association task elicited more anterior brain responses, located further from the sensory-motor cortex, compared to the semantic feature matching task. To do this, we analysed how closely these responses were located to the sensory-motor cortex. Specifically, we classified brain parcels into four groups according to their response to task difficulty: (i) parcels responding only during the semantic association task, (ii) parcels showing responses in both semantic association and non-semantic tasks, (iii) parcels affected in both feature matching and non-semantic tasks, and (iv) parcels responsive exclusively during the feature matching task. We then calculated the shortest distance (global minimum distance) from each parcel to the nearest sensory-motor landmarks for each participant.

We calculated the geodesic distance between each parcel and key landmarks associated with primary visual, auditory and somatomotor cortex. These values were used to identify the minimum geodesic distance to primary sensory-motor regions for each parcel. Three topographical landmarks were used: the central sulcus corresponding to the primary somatosensory/motor cortex; temporal transverse sulcus indicating primary auditory cortex; and calcarine sulcus, marking the location of primary visual cortex. Since the cortical folding patterns vary across participants, and the individual variability in cortical folding increases with cortical surface area[88], both the shapes of these landmarks and the number of vertices within each landmark might show individual differences. We used participant-specific landmark label files to locate the participant-specific vertices belonging to each landmark and participant-specific parcellation to locate the vertices within each parcel.

Geodesic distance along the 'midthickness' of the cortical surface (halfway between the pial and white matter) was calculated using the Connectome Workbench software with an algorithm that measures the shortest path between two vertices on a triangular surface mesh[89,90]. This method returns distance values independent of mesh density. Geodesic distance was extracted from surface geometry (GIFTI) files, following surface-based registration[74]. To ensure that the shortest paths would only pass through the cortex, vertices representing the medial wall were removed from the triangular mesh for this analysis.

We calculated the minimum geodesic distance between each vertex and each landmark. Specifically, for the central sulcus, we calculated the geodesic distance between vertex i outside the central sulcus and each vertex within it (defined for each individual). We then identified vertex j within the central sulcus closest to vertex i, and extracted this value as the minimum geodesic distance for vertex i to this landmark. To compute the minimum geodesic distance for parcel k to the central sulcus, we averaged the minimum distance across all the grayordinate vertices in parcel k to the vertices within the central sulcus. The same procedure was applied to calculate minimum geodesic distance between each parcel and all three sensory-motor landmarks (central sulcus, temporal transverse sulci, and calcarine sulcus). From these three minimum geodesic distances, we selected the lowest distance value (i.e., the closest landmark to parcel k) as the global minimum distance to sensory-motor regions for parcel k. Then we averaged the mean minimum distance of all the parcels within each type of parcels for each participant. Finally, we examined whether mean minimum distance of each type of parcels were different by performing a paired t-test. All p-values are FDR-corrected.

Statistics and reproducibility

We conducted univariate analysis to identify brain regions that responded more strongly to difficult trials in the semantic tasks. For the first level analysis (within-subject), fixed-effects analyses were conducted to estimate the average effects across runs within each subject for each parcel. For the second level analysis (between-subject), we performed random effects analyses to generalize the findings from individual subjects to the larger population. We implemented multiple comparison corrections using the FDR and spin permutation techniques. The FDR correction was applied to control the expected proportion of incorrectly rejected null hypotheses (false discoveries), thereby balancing the need for sensitivity and specificity in our findings. Additionally, the spin permutation correction was utilized to address spatial autocorrelation in neuroimaging data, ensuring that our results are not unduly influenced by the anatomical proximity of analysed regions.

Our study successfully replicated the finding that brain regions supporting controlled retrieval of weak semantic associations are located anteriorly to those involved in matching words based on their visual features within the left inferior frontal gyrus, as identified in prior research (cf. [14]). We extended these findings by demonstrating that similar topographical dissociations are also evident in the medial prefrontal and posterior temporal cortex. This suggests a broader, organized topographical dissociation across the whole brain. Additionally, we replicated the first three connectivity dimensions described by Margulies et al.[18]. We extended these findings by revealing that the two semantic tasks employed in our study rely on distinct connectivity dimensions, thus providing new insights into the neural underpinnings of semantic control.

Reporting summary

Further information on research design is available in the Nature Portfolio Reporting Summary linked to this article.

Data availability

The HCP data is publicly available here https://www.humanconnectome.org/. The York data is not available due to insufficient consent. Researchers wishing to access the data should contact Elizabeth Jefferies or the Chair of the Research Ethics Committee of the York Neuroimaging Centre. Data will be released when this is possible under the terms of the UK GDPR. The numerical source data for graphs are available on Figshare https://doi.org/10.6084/m9.figshare.26104822.v2.

Code availability

Analysis code and source data for figures for this study are available at https://github.com/Xiuyi-Wang/Project_Semantic_Brain_States.

Received: 29 March 2024; Accepted: 24 July 2024;
Published online: 01 August 2024

References

1. Lambon Ralph, M. A., Jefferies, E., Patterson, K. & Rogers, T. T. The neural and computational bases of semantic cognition. *Nat. Rev. Neurosci.* **18**, 42–55 (2017).
2. Xu, Y., Lin, Q., Han, Z., He, Y. & Bi, Y. Intrinsic functional network architecture of human semantic processing: Modules and hubs. *Neuroimage* **132**, 542–555 (2016).
3. Duncan, J. The multiple-demand (MD) system of the primate brain: mental programs for intelligent behaviour. *Trends Cogn. Sci.* **14**, 172–179 (2010).

4. Fedorenko, E., Duncan, J. & Kanwisher, N. Broad domain generality in focal regions of frontal and parietal cortex. *Proc. Natl Acad. Sci. USA* **110**, 16616–16621 (2013).
5. Assem, M., Glasser, M. F., Van Essen, D. C. & Duncan, J. A Domain-General Cognitive Core Defined in Multimodally Parcellated Human Cortex. *Cereb. Cortex* **30**, 4361–4380 (2020).
6. Assem, M., Shashidhara, S., Glasser, M. F. & Duncan, J. Precise Topology of Adjacent Domain-General and Sensory-Biased Regions in the Human Brain. *Cereb. Cortex* **32**, 2521–2537 (2022).
7. Noonan, K. A., Jefferies, E., Visser, M. & Lambon Ralph, M. A. Going beyond inferior prefrontal involvement in semantic control: evidence for the additional contribution of dorsal angular gyrus and posterior middle temporal cortex. *J. Cogn. Neurosci.* **25**, 1824–1850 (2013).
8. Jackson, R. L. The neural correlates of semantic control revisited. *Neuroimage* **224**, 117444 (2021).
9. Gonzalez Alam, T., Murphy, C., Smallwood, J. & Jefferies, E. Meaningful inhibition: Exploring the role of meaning and modality in response inhibition. *Neuroimage* **181**, 108–119 (2018).
10. Gao, Z. et al. Distinct and common neural coding of semantic and non-semantic control demands. *Neuroimage* **236**, 118230 (2021).
11. Wang, X., Margulies, D. S., Smallwood, J. & Jefferies, E. A gradient from long-term memory to novel cognition: Transitions through default mode and executive cortex. *Neuroimage* **220**, 117074 (2020).
12. Chiou, R., Jefferies, E., Duncan, J., Humphreys, G. F. & Lambon Ralph, M. A. A middle ground where executive control meets semantics: the neural substrates of semantic control are topographically sandwiched between the multiple-demand and default-mode systems. *Cereb. Cortex* **33**, 4512–4526 (2023).
13. Greene, A. S., Horien, C., Barson, D., Scheinost, D. & Constable, R. T. Why is everyone talking about brain state? *Trends Neurosci.* **46**, 508–524 (2023).
14. Badre, D., Poldrack, R. A., Paré-Blagoev, E. J., Insler, R. Z. & Wagner, A. D. Dissociable controlled retrieval and generalized selection mechanisms in ventrolateral prefrontal cortex. *Neuron* **47**, 907–918 (2005).
15. Gold, B. T. et al. Dissociation of automatic and strategic lexical-semantics: Functional magnetic resonance imaging evidence for differing roles of multiple frontotemporal regions. *J. Neurosci.* **26**, 6523–6532 (2006).
16. Badre, D. & Wagner, A. D. Left ventrolateral prefrontal cortex and the cognitive control of memory. *Neuropsychologia* **45**, 2883–2901 (2007).
17. Pang, J. C. et al. Geometric constraints on human brain function. *Nature* **618**, 566–574 (2023).
18. Margulies, D. S. et al. Situating the default-mode network along a principal gradient of macroscale cortical organization. *Proc. Natl Acad. Sci. USA* **113**, 12574–12579 (2016).
19. Wang, X. et al. The brain's topographical organization shapes dynamic interaction patterns that support flexible behaviour based on rules and long term knowledge. *J. Neurosci.* **44**, e2223232024 (2024).
20. Bolt, T. et al. A parsimonious description of global functional brain organization in three spatiotemporal patterns. *Nat. Neurosci.* **25**, 1093–1103 (2022).
21. Raichle, M. E. The Brain's Default Mode Network. *Annu Rev. Neurosci.* **38**, 433–447 (2015).
22. Smallwood, J. et al. The default mode network in cognition: a topographical perspective. *Nat. Rev. Neurosci.* **22**, 503–513 (2021).
23. Vatansever, D., Menon, D. K. & Stamatakis, E. A. Default mode contributions to automated information processing. *Proc. Natl Acad. Sci. USA* **114**, 12821–12826 (2017).
24. Schacter, D. L. et al. The Future of Memory: Remembering, Imagining, and the Brain. *Neuron* **76**, 677–694 (2012).
25. Davey, J. et al. Exploring the role of the posterior middle temporal gyrus in semantic cognition: Integration of anterior temporal lobe with executive processes. *Neuroimage* **137**, 165–177 (2016).
26. Konishi, M., Mclaren, D. G., Engen, H. & Smallwood, J. Shaped by the Past: The Default Mode Network Supports Cognition that Is Independent of Immediate Perceptual Input. *PLoS One* **10**, e0132209 (2015).
27. Smallwood, J. et al. Escaping the here and now: Evidence for a role of the default mode network in perceptually decoupled thought. *Neuroimage* **69**, 120–125 (2013).
28. Luppi, A. I. et al. A synergistic core for human brain evolution and cognition. *Nat. Neurosci.* **25**, 771–782 (2022).
29. Luppi, A. I., Rosas, F. E., Mediano, P. A. M., Menon, D. K. & Stamatakis, E. A. Information decomposition and the informational architecture of the brain. *Trends Cogn. Sci.* **28**, 352–368 (2024).
30. Wang, X., Gao, Z. & Smallwood, J. Both Default and Multiple-Demand Regions Represent Semantic Goal Information. *J. Neurosci.* **41**, 3679–3691 (2021).
31. Mckeown, B. et al. The relationship between individual variation in macroscale functional gradients and distinct aspects of ongoing thought. *Neuroimage* **220**, 117072 (2020).
32. Shao, X. et al. Individual differences in gradients of intrinsic connectivity within the semantic network relate to distinct aspects of semantic cognition. *Cortex* **150**, 48–60 (2022).
33. Cole, M. W. et al. Multi-task connectivity reveals flexible hubs for adaptive task control. *Nat. Neurosci.* **16**, 1348–1355 (2013).
34. Shine, J. M. et al. Human cognition involves the dynamic integration of neural activity and neuromodulatory systems. *Nat. Neurosci.* **22**, 289–296 (2019).
35. Finc, K. et al. Dynamic reconfiguration of functional brain networks during working memory training. *Nat. Commun.* **11**, 2435 (2020).
36. Khambhati, A. N., Medaglia, J. D., Karuza, E. A., Thompson-Schill, S. L. & Bassett, D. S. Subgraphs of functional brain networks identify dynamical constraints of cognitive control. *PLoS Comput Biol.* **14** https://doi.org/10.1371/journal.pcbi.1006234 (2018).
37. Koch, C., Massimini, M., Boly, M. & Tononi, G. Neural correlates of consciousness: Progress and problems. *Nat. Rev. Neurosci.* **17**, 307–321 (2016).
38. Wang, X. et al. The structural basis of semantic control: Evidence from individual differences in cortical thickness. *Neuroimage* **181**, 480–489 (2018).
39. Zhang, M. et al. Knowing what you need to know in advance: The neural processes underpinning flexible semantic retrieval of thematic and taxonomic relations. *Neuroimage* **224**, 117405 (2021).
40. González-García, C., Flounders, M. W., Chang, R., Baria, A. T. & He, B. J. Content-specific activity in frontoparietal and default-mode networks during prior-guided visual perception. *Elife*. **7**, https://doi.org/10.7554/eLife.36068 (2018).
41. Gao, Z. et al. Flexing the principal gradient of the cerebral cortex to suit changing semantic task demands. *Elife* **11**, https://doi.org/10.7554/eLife.80368 (2022).
42. Chiou, R. & Lambon Ralph, M. A. Task-Related Dynamic Division of Labor Between Anterior Temporal and Lateral Occipital Cortices in Representing Object Size. *J. Neurosci.* **36**, 4662–4668 (2016).
43. Glasser, M. F. et al. The minimal preprocessing pipelines for the Human Connectome Project. *Neuroimage* **80**, 105–124 (2013).
44. Dale, A. M. Optimal Experimental Design for Event-Related FMRI. *Hum. Brain Mapping* **8**, 109–114 (1999).
45. Fedorenko, E., Behr, M. K. & Kanwisher, N. Functional specificity for high-level linguistic processing in the human brain. *Proc. Natl Acad. Sci.* **108**, 16428–16433 (2011).
46. Barch, D. M. et al. Function in the human connectome: Task-fMRI and individual differences in behavior. *Neuroimage* **80**, 169–189 (2013).
47. Faskowitz, J., Esfahlani, F. Z., Jo, Y., Sporns, O. & Betzel, R. F. Edge-centric functional network representations of human cerebral cortex reveal overlapping system-level architecture. *Nat. Neurosci.* **23**, 1644–1654 (2020).

48. Sporns, O., Faskowitz, J., Teixeira, A. S., Cutts, S. A. & Betzel, R. F. Dynamic expression of brain functional systems disclosed by fine-scale analysis of edge time series. *Netw. Neurosci.* **5**, 405–433 (2021).
49. Esteban, O. et al. fMRIPrep: a robust preprocessing pipeline for functional {MRI}. *Nat. Methods* **16**, 111–116 (2018).
50. Gorgolewski, K. et al. Nipype: a flexible, lightweight and extensible neuroimaging data processing framework in Python. *Front Neuroinform* **5**, 13 (2011).
51. Tustison, N. J. et al. N4ITK: Improved N3 Bias Correction. *IEEE Trans. Med Imaging* **29**, 1310–1320 (2010).
52. Avants, B. B., Epstein, C. L., Grossman, M. & Gee, J. C. Symmetric diffeomorphic image registration with cross-correlation: Evaluating automated labeling of elderly and neurodegenerative brain. *Med Image Anal.* **12**, 26–41 (2008).
53. Zhang, Y., Brady, M. & Smith, S. Segmentation of brain MR images through a hidden Markov random field model and the expectation-maximization algorithm. *IEEE Trans. Med Imaging* **20**, 45–57 (2001).
54. Dale, A. M., Fischl, B. & Sereno, M. I. Cortical Surface-Based Analysis: I. Segmentation and Surface Reconstruction. *Neuroimage* **9**, 179–194 (1999).
55. Klein, A. et al. Mindboggling morphometry of human brains. *PLoS Comput Biol.* **13**, e1005350 (2017).
56. Fonov, V. S., Evans, A. C., McKinstry, R. C., Almli, C. R. & Collins, D. L. Unbiased nonlinear average age-appropriate brain templates from birth to adulthood. *Neuroimage* **47**, S102 (2009).
57. Evans, A. C., Janke, A. L., Collins, D. L. & Baillet, S. Brain templates and atlases. *Neuroimage* **62**, 911–922 (2012).
58. Greve, D. N. & Fischl, B. Accurate and robust brain image alignment using boundary-based registration. *Neuroimage* **48**, 63–72 (2009).
59. Jenkinson, M., Bannister, P., Brady, M. & Smith, S. Improved Optimization for the Robust and Accurate Linear Registration and Motion Correction of Brain Images. *Neuroimage* **17**, 825–841 (2002).
60. Cox, R. W. & Hyde, J. S. Software tools for analysis and visualization of fMRI data. *NMR Biomed.* **10**, 171–178 (1997).
61. Power, J. D. et al. Methods to detect, characterize, and remove motion artifact in resting state fMRI. *Neuroimage* **84**, 320–341 (2014).
62. Behzadi, Y., Restom, K., Liau, J. & Liu, T. T. A component based noise correction method (CompCor) for BOLD and perfusion based fMRI. *Neuroimage* **37**, 90–101 (2007).
63. Satterthwaite, T. D. et al. An improved framework for confound regression and filtering for control of motion artifact in the preprocessing of resting-state functional connectivity data. *Neuroimage* **64**, 240–256 (2013).
64. Lanczos, C. Evaluation of Noisy Data. *J. Soc. Ind. Appl. Math. Ser. B Numer. Anal.* **1**, 76–85 (1964).
65. Abraham, A. et al. Machine learning for neuroimaging with scikit-learn. *Front. Neuroinform.* **8**, https://doi.org/10.3389/fninf.2014.00014 (2014).
66. Ciric, R. et al. Mitigating head motion artifact in functional connectivity MRI. *Nat. Protoc.* **13**, 2801–2826 (2018). *2018 13:12*.
67. Pedregosa Fabianpedregosa, F. et al. Scikit-learn: Machine Learning in Python Gaël Varoquaux Bertrand Thirion Vincent Dubourg Alexandre Passos PEDREGOSA, VAROQUAUX, GRAMFORT ET AL. Matthieu Perrot. *J. Mach. Learn. Res.* **12**, 2825–2830 (2011).
68. Kong, R. et al. Individual-Specific Areal-Level Parcellations Improve Functional Connectivity Prediction of Behavior. *Cereb. Cortex* **31**, 4477–4500 (2021).
69. Harris, C. R. et al. Array programming with NumPy. *Nature* **585**, 357–362 (2020).
70. Fischl, B., Sereno, M. I. & Dale, A. M. Cortical surface-based analysis: II. Inflation, flattening, and a surface-based coordinate system. *Neuroimage* **9**, 195–207 (1999).
71. Dale, A. M., Fischl, B. & Sereno, M. I. Cortical Surface-Based Analysis. *Neuroimage* **9**, 179–194 (1999).
72. Salimi-Khorshidi, G. et al. Automatic denoising of functional MRI data: Combining independent component analysis and hierarchical fusion of classifiers. *Neuroimage* **90**, 449–468 (2014).
73. Glasser, M. F. et al. Using temporal ICA to selectively remove global noise while preserving global signal in functional MRI data. *Neuroimage* **181**, 692–717 (2018).
74. Robinson, E. C. et al. MSM: A new flexible framework for Multimodal Surface Matching. *Neuroimage* **100**, 414–426 (2014).
75. Mueller, S. et al. Individual Variability in Functional Connectivity Architecture of the Human Brain. *Neuron* **77**, 586–595 (2013).
76. Braga, R. M. & Buckner, R. L. Parallel Interdigitated Distributed Networks within the Individual Estimated by Intrinsic Functional Connectivity. *Neuron* **95**, 457–471.e5 (2017).
77. Gordon, E. M. et al. Precision Functional Mapping of Individual Human Brains. *Neuron* **95**, 791–807.e7 (2017).
78. Laumann, T. O. et al. Functional System and Areal Organization of a Highly Sampled Individual Human Brain. *Neuron* **87**, 657–670 (2015).
79. Kong, R. et al. Spatial Topography of Individual-Specific Cortical Networks Predicts Human Cognition, Personality, and Emotion. *Cereb. Cortex* **29**, 2533–2551 (2019).
80. Fair, D. A. et al. Development of distinct control networks through segregation and integration. *Proc. Natl Acad. Sci.* **104**, 13507–13512 (2007).
81. Cui, Z. et al. Individual Variation in Functional Topography of Association Networks in Youth. *Neuron* **106**, 340–353.e8 (2020).
82. Cohen, A. L. et al. Defining functional areas in individual human brains using resting functional connectivity MRI. *Neuroimage* **41**, 45–57 (2008).
83. Schaefer, A. et al. Local-Global Parcellation of the Human Cerebral Cortex from Intrinsic Functional Connectivity MRI. *Cereb. Cortex* **28**, 3095–3114 (2018).
84. Gordon, E. M. et al. Generation and Evaluation of a Cortical Area Parcellation from Resting-State Correlations. *Cereb. Cortex* **26**, 288–303 (2016).
85. Thomas Yeo, B. T. et al. The organization of the human cerebral cortex estimated by intrinsic functional connectivity. *J. Neurophysiol.* **106**, 1125–1165 (2011).
86. Burt, J. B., Helmer, M., Shinn, M., Anticevic, A. & Murray, J. D. Generative modeling of brain maps with spatial autocorrelation. *Neuroimage* **220**, 117038 (2020).
87. Vos de Wael, R. et al. BrainSpace: a toolbox for the analysis of macroscale gradients in neuroimaging and connectomics datasets. *Commun. Biol.* **3**, 1–10 (2020).
88. Van Essen, D. C. et al. Cerebral cortical folding, parcellation, and connectivity in humans, nonhuman primates, and mice. *Proc. Natl Acad. Sci. USA* **116**, 26173–26180 (2019).
89. Mitchell, J. S. B., Mount, D. M. & Papadimitriou, C. H. Discrete Geodesic Problem. *SIAM J. Comput.* **16**, 647–668 (1987).
90. O'Rourke, J. Computational geometry column 35. *ACM SIGACT N.* **30**, 31–32 (1999).

Acknowledgements

We are grateful to Pradeepa Ruwan and Antonia De Freitas for piloting the experiment. X. W. discloses support for the research of this work from Scientific Foundation of Institute of Psychology, Chinese Academy of Sciences (Grant Number E1CX4725CX) and the National Natural Science Foundation of China (Grant Number 32300881). Y.D. discloses support for the publication of this work from the STI 2030—Major Projects (Grant Number 2021ZD0201500), the National Natural Science Foundation of China (Grant Number 31822024), and Scientific Foundation of Institute of Psychology, Chinese Academy of Sciences (Grant Number E2CX3625CX). The research was supported by a European Research Council Consolidator grant (Project ID: 771863 - FLEXSEM) to E.J.

Author contributions

X.W., E.J. designed research; K.K.R., and X.W. collected the data, X.W. analyzed data; X.W., Y.D., and E.J. wrote the original manuscript. All authors edited the manuscript.

Competing interests

The authors declare no competing interests.

Additional information

Supplementary information The online version contains supplementary material available at https://doi.org/10.1038/s42003-024-06630-7.

Correspondence and requests for materials should be addressed to Xiuyi Wang, Yi Du or Elizabeth Jefferies.

Peer review information *Communications Biology* thanks Veronica Diveica and the other, anonymous, reviewer(s) for their contribution to the peer review of this work. Primary Handling Editor: Benjamin Bessieres. A peer review file is available.